2012

Using Structural Analysis to Assess Possible Formation Mechanisms of the Gneiss Domes of the Harvey Cardiff Domain, Eastern Ontario

Callie Sendek
Scripps College

Using structural analysis to assess possible formation mechanisms of the gneiss domes of the Harvey Cardiff Domain, eastern Ontario

Callie Sendek

Pomona College Geology Department

Senior thesis submitted in partial satisfaction of the requirements for B.A. degree in Geology at Scripps College

April 20, 2012

Advisor: Linda Reinen

Second Reader: Robert Gaines

Abstract

Gneiss domes are structural features associated with orogens worldwide. This study provides a structural analysis of the domes of the Harvey Cardiff Domain, associated with the Grenville Orogeny. Structural data and oriented samples were collected during field work in the summer of 2012. These were used in combination with published and unpublished foliation and lineation data to analyze structural patterns and determine a mechanism of formation for the domes. The end member scenarios for dome formation were taken from the gneiss dome classification scheme devised by Yin (2004). Most of these mechanisms were eliminated based on a lack of necessary large scale geologic features in the region of the study area. An analysis of the foliation pattern of the Cheddar and Cardiff domes was most consistent with formation by diapirism. However, the foliation patterns of the domes differ from the expected diapiric pattern, and seems to represent a non-horizontal slice through a diapir, cutting through a diapir neck in the north and a diapir hat in the south. This pattern can also be explained by rotation of diapiric foliation due to strain induced by the main orogenic event. This hypothesis was tested using COMSOL, a finite elastic strain model, and found to be realistic. With the methods used in this study it is not possible to tell whether this rotation occurred after or during dome emplacement.

Table of Contents

Table of Figures

Table of Tables

1. Introduction

Gneiss domes are structures associated with major orogenic events worldwide. They are broadly defined as circular to oval-shaped metamorphic-plutonic cores overlain by a mantle of supracrustal rocks containing domal contact parallel layering. Early research on gneiss domes cited magmatism and the effects of density inversions as the driving forces behind dome formation and emplacement (e.g. Eskola, 1949; Fletcher, 1972; Gilbert and Merle, 1987). More recent studies have widened the list of possible formation mechanisms to include those associated with faulting. The extent of current research has lead to the development of a classification scheme linking the physical characteristics of domes and dome systems to their mechanism of formation (Yin, 2004). Domes are often formed in dynamic environments where changing stress and strain patterns coalesce to develop their structures. This complicates the process of making conclusions about strain paths from finite strain patterns recorded in dome rocks. Nonetheless, different processes of development do correlate with distinctive structural geometries. This study uses structural analyses of the gneiss domes of the Harvey Cardiff Domain of the Grenville Province in Eastern Ontario to assess the possible mechanisms that lead to their formation.

Yin's framework serves as a guide of idealized, end member cases of dome formation mechanisms (Fig. 1). Her characterization of individual domes begins with the broad categories of fault-unrelated and fault related. More specific subcategories of fault unrelated domes include those produced by magmatism, contrasts in mechanical rock properties, and superposition of multiple folding events. Fault related domes can be associated with detachment faulting, thrusting, strike slip shear zones, or ductile shear zones. Each of these types contains end member scenarios demonstrating how creation takes place. Association with large-scale geologic features, structural patterns, and kinematic indicators aids in distinguishing between the above mechanisms. This makes observations of structural features of all sizes, from map scale to microscale, critical in understanding dome formation.

The spacing relationship between gneiss domes in a dome complex also provides insight into mechanisms of formation (Yin, 2004). A separate classification scheme presents the different spacing possibilities (Fig. 2). Dome systems are initially differentiated into linear and nonlinear arrays, and then divided further into evenly spaced and unevenly spaced. Although spacing pattern is not diagnostic it is helpful in confirming hypotheses of formation mechanisms formed during the study of individual domes.

The Grenville Province of eastern Canada (Fig. 3) is defined by the metamorphic signature of the Grenville Orogeny of the late Mesoproterozoic to early Neoproterozoic (1090 to 980 Ma)

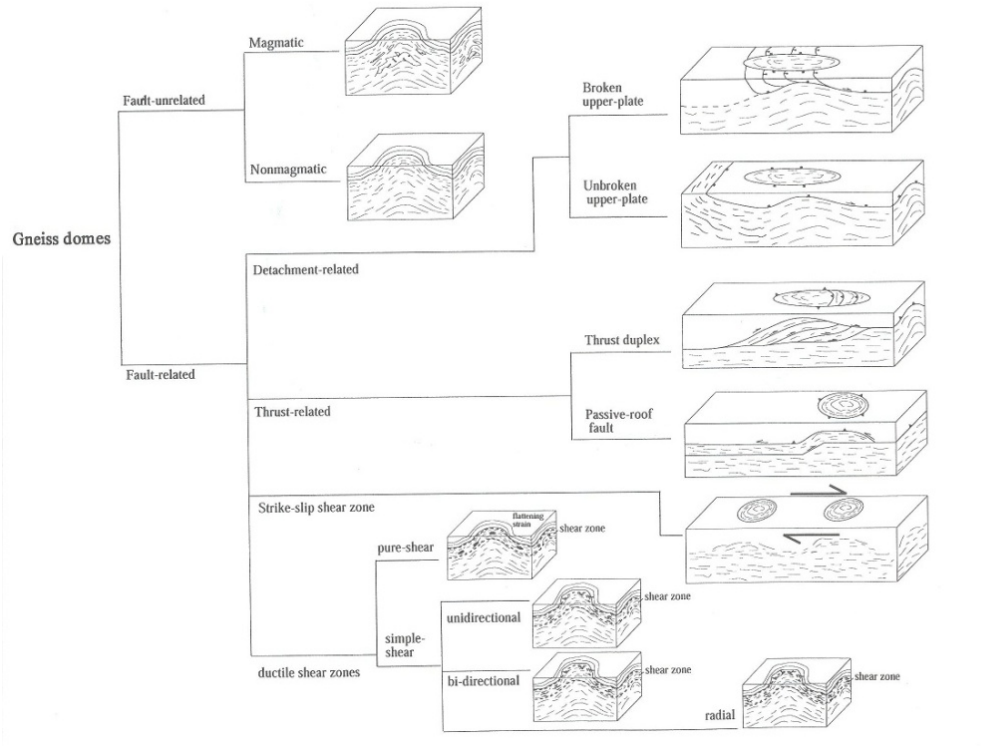

Figure 1: Gneiss Dome Classification Scheme. Schematic gneiss dome classification system showing idealized, end member cases of dome formation mechanisms. *From Yin, 2004.*

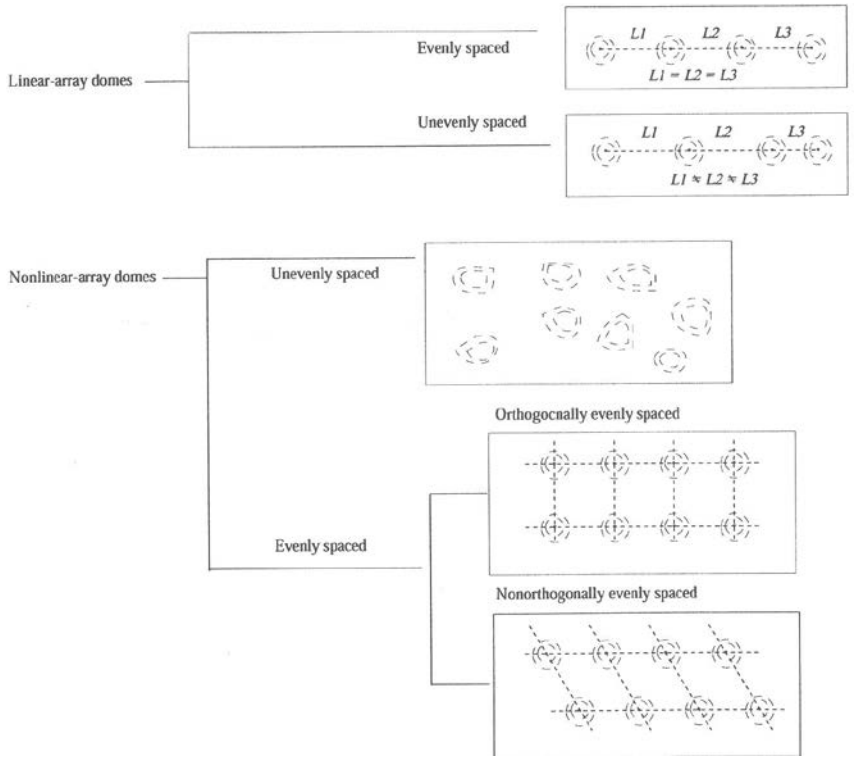

Figure 2: Gneiss Dome System Classification Scheme. (*From Yin, 2004)*.

(e.g. Carr et al., 2000; Rivers, 2008). The province extends along the eastern coast of North America, from the United States border to Labrador. However, the orogen affected a much larger region where Grenvillian rocks exist mostly in the subsurface. This region includes the eastern and southwestern United States, Mexico, and the United Kingdom (Darabi and Piper, 2004). The province was amalgamated and metamorphosed in a series of accretionary and collisional events, culminating in the collision of Laurentia and Amazonia (Rivers, 2008; Hanmer et al. 2000). Within this single event, pulses of collision and extension are recorded (Rivers, 1997). After almost a billion years of erosion, the rock exposed at the surface today represents the mid to lower crustal levels of the orogeny (Cosca et al., 1995). Although subsequent orogenies have occurred on the east coast of Laurentia, they did not lead to widespread recrystallization in the Grenville Province. Therefore, the metamorphic rocks of the province act as a record of Grenvillian tectonic evolution, and provide the longest continuous example of a Late Mesoproterozoic orogenic belt in the world (Tollo et al., 2004).

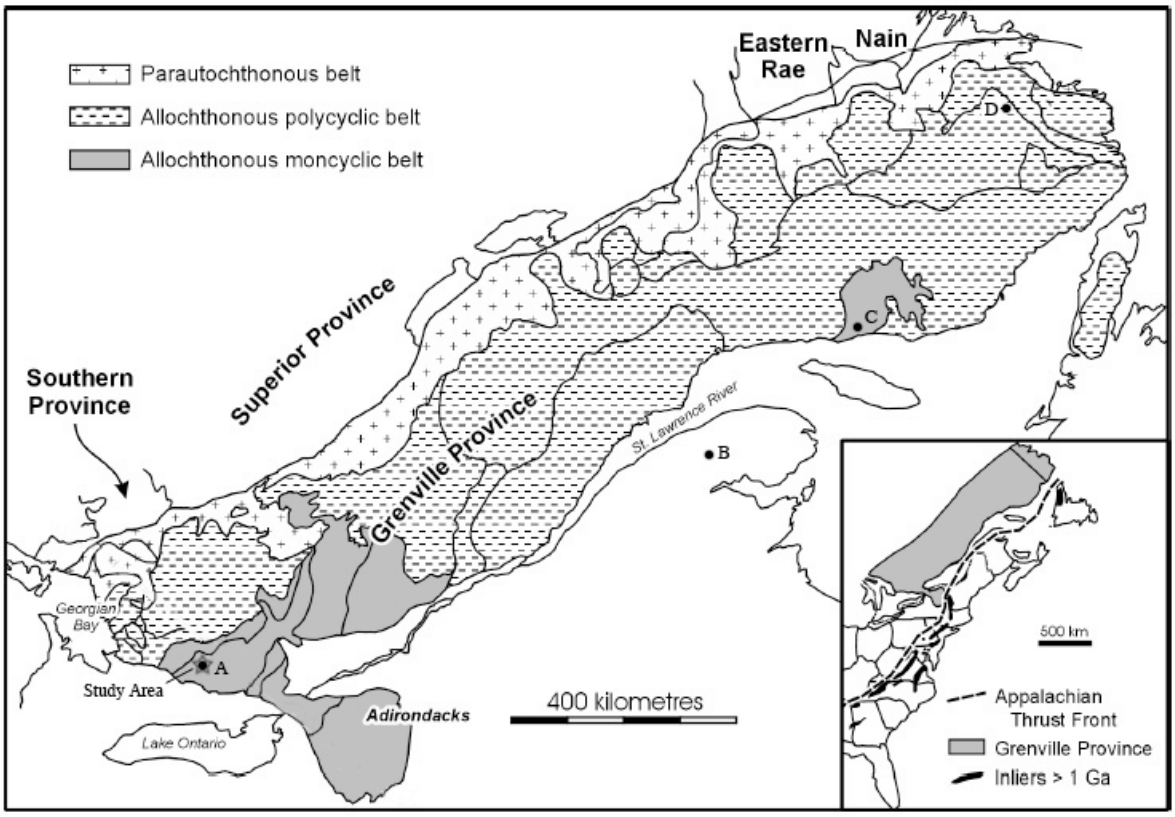

Figure 3: The Grenville Province of Eastern Canada. Study area marked with a star. Dots are locations of gneiss dome complexes: (A) Faraday Dome, Cardiff Dome, Cheddar Dome, Anstruther Dome, and Burleigh Dome (B) Lemieux Dome, and Renia Dome (C) Watshishou Dome, Pontbriand Dome, and Jalobert Dome (D) two unnamed domes. *(Modified from Carr et al., 2000).*

Several gneiss dome complexes have been identified in the Grenville Province. Figure 3 shows a map of the domes within the Grenville as compiled in Whitney et al. (2004). The gneiss domes of the Harvey Cardiff are the farthest south, and will be described in detail in subsequent paragraphs. There are two recognized sets of domes in Québec. Two domes, the Lemieux Dome and the Renia Dome, have been identified on the Gaspé Penninsula. The Lemieux Dome is unusual in that it is composed of uplifted sedimentary and volcanic rocks, rather than granitic gneiss. However, it has been included in gneiss dome literature because of the suggestion that the domal structure was produced by upwelling of granitic intrusions. This dome is not associated with the Grenville orogeny, as the warped sediments are Siluro-Devonian, significantly younger than the Grenville Orogen (McNeice et al., 1991). A complex of three domes lies on the northeastern coast of Québec: the Watshishou Dome, the Pontbriand Dome, and the Jalobert Dome. These domes are cored by orthogneisses containing dated monzonite that place their metamorphism during the Grenville. An analysis of their structures has recently attributed their formation to diapirism, although older studies cite polyphase folding (Gervais et al., 2004). Finally, two unnamed domes are present in Labrador. They lack published work regarding their formation (Whitney et al., 2004). This study of the Harvey Cardiff domes will add to the scarce information on Grenville gneiss domes and allow comparison of orogenic conditions between the Harvey Cardiff and other areas with studied gneiss dome complexes.

The southern portion of the Grenville Province can be broken down into three main lithotectonic masses (Fig. 4) that formed independently before their accretion (Carr et al., 2000). The westernmost extent of the Province is the Central Gneiss Belt (CGB), which formed the Pre-Grenvillian margin of Laurentia. The rocks of the CGB date from before 1450 Ma and were strongly deformed and transported to the northwest during the orogen. The CGB is separated from the Central Metasedimentary Belt (CMB) to the east by the Central Metasedimentary Belt boundary thrust zone (CMBbtz), an upper amphibolite facies, SE dipping ductile shear zone with a tops to the NW sense of shear. The CMB is an amalgamated series of back arc terranes originally comprised of marine sedimentary rocks. The timing of the accretion of these arcs to the CGB is disputed; with some advocating for accretion before 1.4 Ga (Hanmer et al., 2000), and some arguing that the arcs joined the continent only shortly before the main orogeny took place around 1.1 Ga (Timmerman et al., 1997). Further east is the Frontenac-Adirondack Belt (FAB), a younger group of lithotectonic domains that show a distinct structural, metamorphic, and magmatic history. The FAB was amalgamated onto the CMB between 1170 and 1160 Ma. The CMB can be further divided into domains based on differences in magmatic signatures. Each one formed in isolation before amalgamation and accretion (Easton and Kamo, 2011).

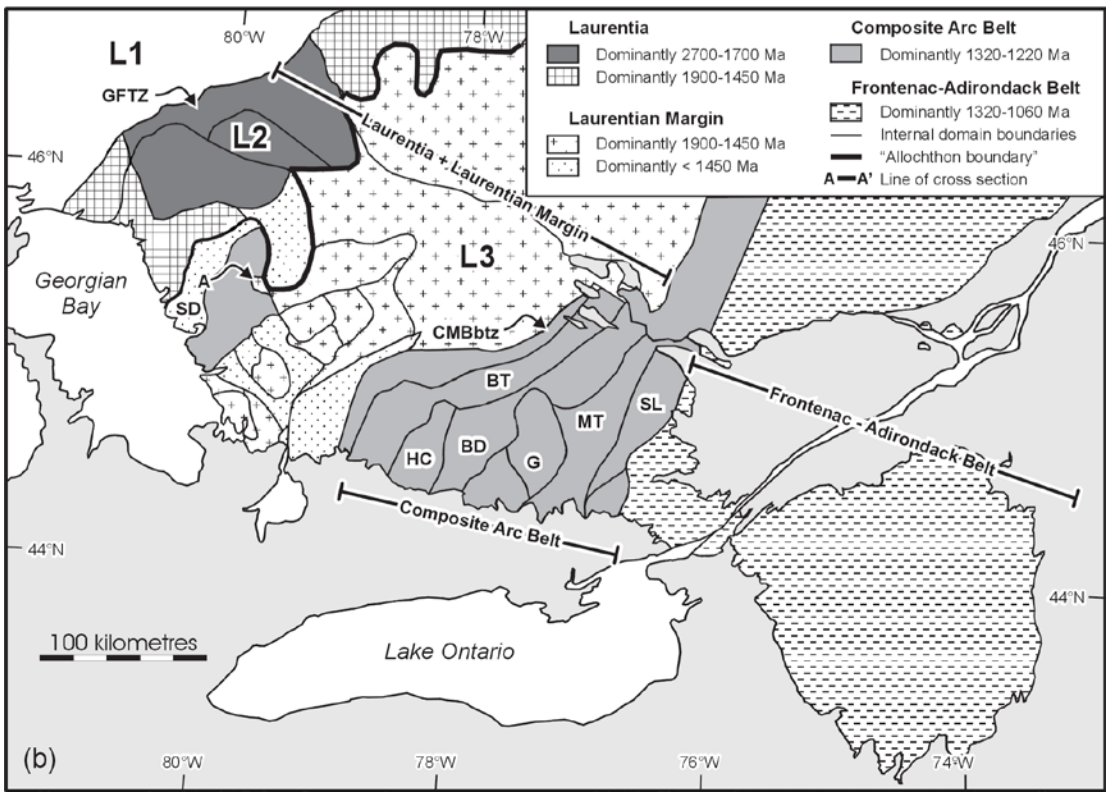

Figure 4: Main Lithotectonic Masses of the Southern Grenville. The three main lithotectonic masses of the southern Grenville Province: The Laurentian Margin, also called the Central Gneiss Belt (CGB), Central Metasedimentary Belt (CMB) Frontenac-Adirondak Belt (FAB). Also pictured are the subdomains of the CMB: Central Metasedimentary Belt Boundary Thrust Zone (CMBbtz), Belmont Terrane (BT), Harvey Cardiff Domain (HC), Grimsthorpe Domain (G), Mazinaw Domain (MT), Sharbot Lake Domain (SL). The gneiss dome complex spans the entire Harvey Cardiff Domain (*Modified from Carr et al., 2000).*

The Harvey-Cardiff Domain (Fig. 4) differs from other CMB domains due to the presence of several gneiss cored structural domes, which have been interpreted as gneiss domes (e.g. Bright, 1987). Five domes have been identified within the domain (Fig. 5). They lie in a line trending roughly northeast-southwest. From north to south they are: the Faraday Dome, the Cardiff Dome, the Cheddar Dome, the Anstruther Dome, and the Burleigh Dome. Although mapped by the Ontario Geologic Society as a gneiss dome, the Faraday Dome does not meet the criteria of a circular shape with a clear core and mantle, and has thus been excluded from this study.

This study focuses on the Cardiff and Cheddar Domes, but includes the Anstruther and Burleigh Domes in an analysis of the gneiss dome system. The Cardiff Dome lies to the north and has a less distinct core and mantle geometry than the southern three domes. Two major types of rock form the dome: amphibole and pyroxene rich fenite and granitic gneiss. Rather than forming a distinct mantle and core structure, the fenite appears entrained within the granitic gneiss body. The granitic gneiss dates between 1250 and 1240 Ma, and is composed of laminated metaluminous to marginally peraluminous alaskite and leucocratic monzogranite. Within these

units are highly syenitized rocks with patches and veins of alkali pyroxene and amphibole. Surrounding the main dome are gneissic tonalities, trondhjemites, and granodiorites along with medium to coarse grained calcitic marble containing 20-60% silicious impurities (Lumbers and Vertolli, 2003).

The Cheddar Dome is cored by alaskite from the same pulse of magmatism as them alaskite of the Cardiff Dome core to the north. The core rocks have laminated structure and metamorphic fabrics. These are intruded by late pegmatites of the Fenite-Carbonatite Suite of 1070 to 1040 Ma. Pegmatites are red and pink, quartz-alkali feldspar pegmatite dikes. The most heavily sampled mantle rocks were amphibole rich metasedimentary rocks. Marbles are the predominant rock type in contact with the Cheddar core gneiss, particularly on the western side. The marbles are medium to coarse grained and contain 20 to 60% siliceous impurities. Skarns developed from this calcitic marble are also present, and contain mixtures of diopside, amphibole, epidote, titanite, garnet, potassium feldspar, scapolite, calcite and quartz. Micaceous sandy metasedimentary rocks derived from greywacke and siltstone are common in the southern mantle (Lumbers and Vertolli, 2000a).

The Anstruther and Burleigh Domes have a similar geologic makeup, despite differences in geometry. The cores are made primarily of gneissic trondhjemite and granodiorite units, dating between 1280 and 1270 Ma. Core units display a laminated structure and veins of coarse-grained quartzofeldspathic material. Also within the core are discrete units of felsic alaskite intrusives. They are metaluminous to slightly paraluminous with augen structures and relict igneous textures. The domes are mantled primarily by calcitic marble (Lumbers and Vetrolli, 2000a; Lumbers and Vetrolli, 2000b).

Structural analysis of the Cardiff and Cheddar domes, as well as the entire Harvey Cardiff gneiss dome system, will determine possible formation mechanisms of the gneiss domes. Different mechanisms require distinct settings and stress states for dome growth to occur. Thus, by determining domal formation mechanisms, this study aims to provide insight into the stress state on the edge of the CMB during the time of the orogeny. Conclusions about the Harvey Cardiff Domes can be used in comparison with other studied gneiss domes in the Grenville, particularly those that have been studied thoroughly in Québec. The study also addresses the question of how the stress fields in an orogenic event may rotate and overprint foliations left by dome formation. This is a question not addressed to date in gneiss dome literature.

Figure 5: Geologic Map of the Harvey Cardiff Gneiss Dome Complex. (*Base map from Ontario Geologic Survey).*

2. Methods

2.1 Sample and Structural Data Collection

I collected structural data and oriented samples during a two week field session in the summer of 2011. I used a Brunton field compass to measure the strikes and dips of foliation and trends and plunges of lineation. Observed foliations are both compositional and tectonic. Observed lineations are aligned mineral grains, fold hinges, and boudin necks. Structural measurements are from sites in both the mantle and the core of the Cheddar Dome (See Appendix A for a full list of field measurements). I collected a suite of oriented samples to provide a complete picture of the range of geology of the dome (See Appendix B for full list of oriented samples). Twenty seven samples are from fourteen sites (Fig. 6). They represent the alaskite gneiss and pegmatites of the core, as well as the amphibolites and marble of the mantle. I oriented samples by drawing strike and dip markers in situ and recording their orientations as measured using a Brunton compass. Where mineral lineations were present at the site, their orientations were drawn directly on to the rock sample when possible. This was usually aided by the fact that lineations occur primarily on foliation planes, which most samples contained.

2.2 Thin Section Analysis

I cut thin sections from collected samples along the structural plane, perpendicular to foliation and parallel to lineation, where present. Thin sections are marked with a notch in the upper northwest corner, when possible, to ensure that the orientations of the sections were clear. Thin sections were made from samples with and without lineations. I analyzed the thin sections for three types of information: composition, fabric analysis, and shear sense indicators. I determined composition and performed fabric analyses using a petrographic microscope. Finally, I analyzed the thin sections for sense of shear indicators including quartz ribbons, core and mantle structures in feldspar grains, mica fish, and rigid grain rotation.

2.3 Creation of Map

I collected structural measurements at 16 sites during the field session and mapped them using ArcGIS, adding them to a compilation of field data put together by Nick Culsahw which included field data he collected between 1977-79, as well as data from Hewitt (1957) and Culshaw (1981). I scanned this data compilation a hard copy map, georeferenced it, and created a database of structural information by digitizing lineation and foliation measurements. For the purpose of this study, only tectonic foliations, compositional foliations, mineral stretching lineations, and c-axis orientation of quartz grain measurements are included.

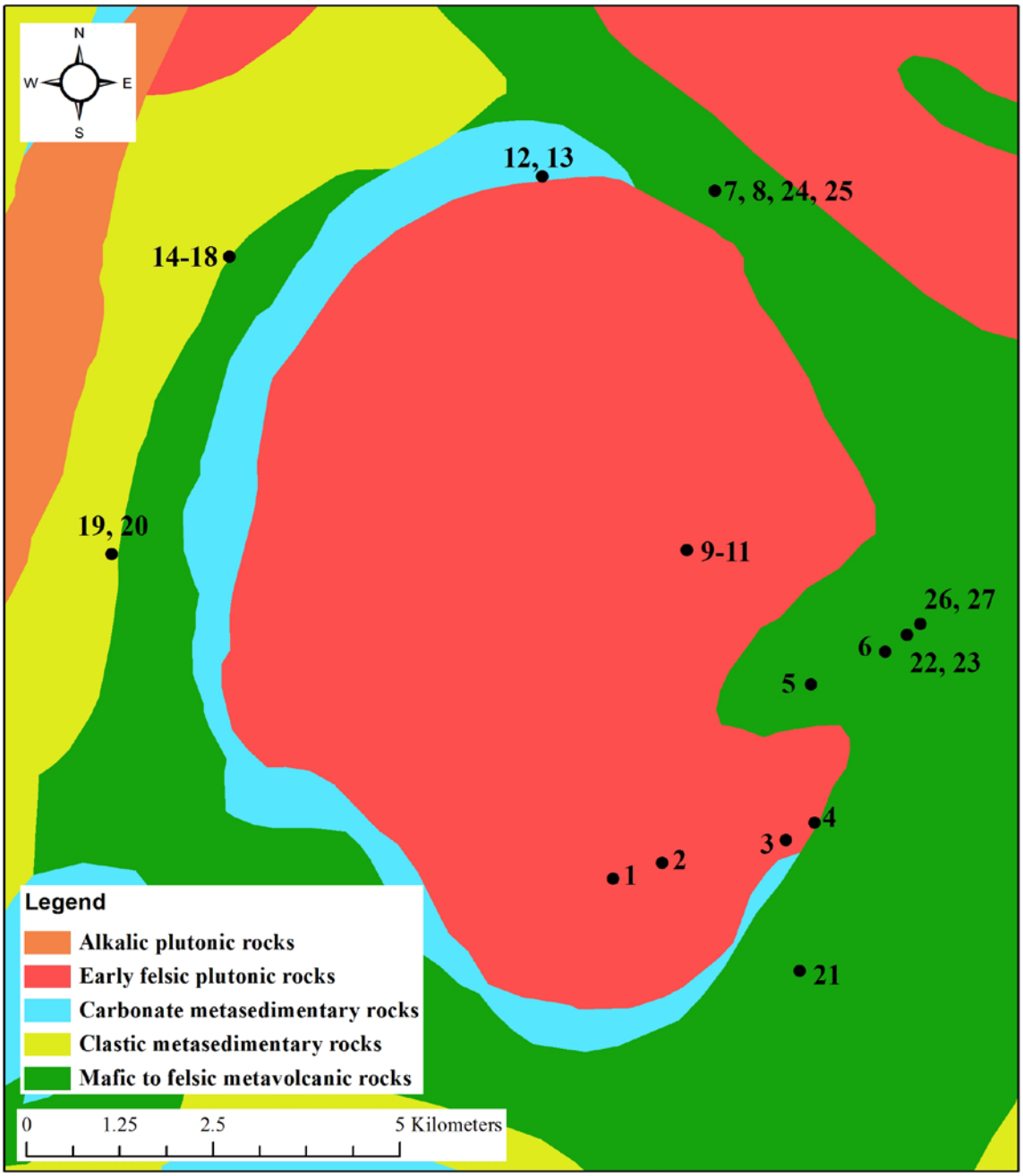

Figure 6: Sample Sites. Sample sites around the Cheddar Dome, numbers correspond to oriented samples taken at each location. (*Base map from Ontario Geologic Survey).*

2.4 Consideration of Formation Mechanisms

I considered each of the formation mechanisms mentioned in Yin (2004) in light of the large scale geologic setting of the Harvey-Cardiff domes. Several can be ruled out due to the absence of key features associated with gneiss dome production by that method. This analysis is described in section 3.1 below.

2.5 Analysis of Cheddar and Cardiff Dome Structures

I plotted foliation data on stereonets using Stereonet 32 (free software, copyright Dr. K. Roeller, available at http://www.ruhr-uni-bochum.de/hardrock/downloads.html) and contoured them in seven intervals using cosine sums as the density calculation. Foliation data for the region of the Cardiff and Cheddar domes show a dominant foliation trend striking 070 (Fig. 7). In order to make other structural patterns apparent, I removed the foliations striking thirty degrees to either side of this orientation (40-100) from data sets. The domes were then divided into regions based on foliation patterns (I-VII in Figures 18 and 21). Each region is accompanied by a contoured stereonet plot and rose diagram of foliation dip direction. Lineations in both domes are also plotted on a contour stereonet and included in analysis. I compared these patterns to expected structural patterns from the narrowed list of possible formation mechanisms.

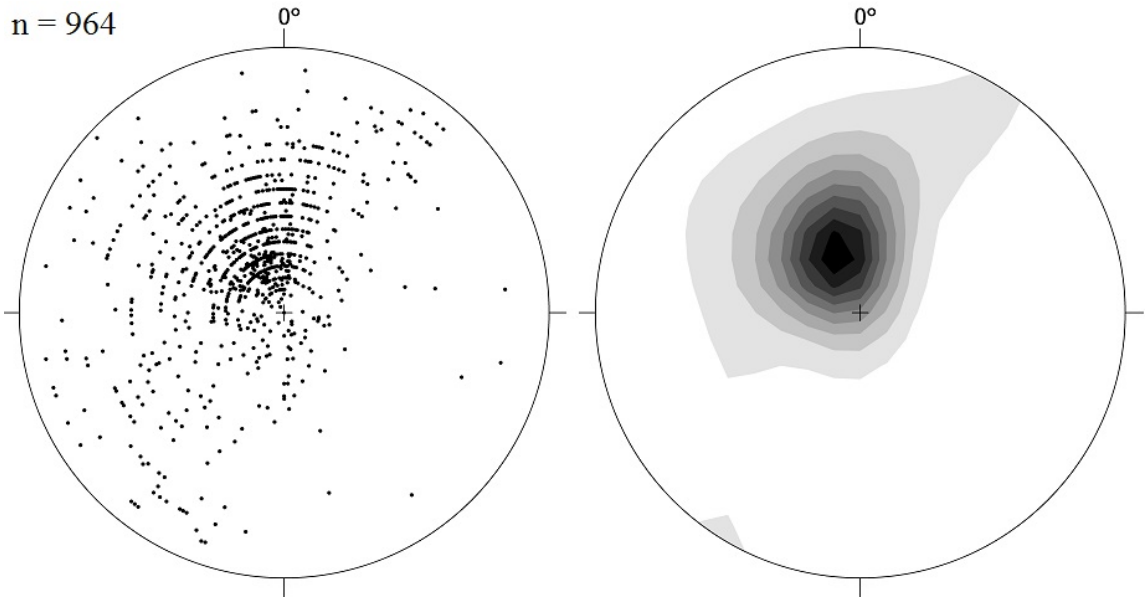

Figure 7: Dominant Regional Foliation Trend. Stereonet and contour plot of poles to foliation planes in the Cheddar and Cardiff Dome regions. The foliation data have a maxima oriented 070/64.

2.6 COMSOL Modeling

I used COMSOL Multiphysics (www.comsol.com) to constrain timing of dome formation in relation to the major orogenic collision by analyzing how expected foliation patterns for dome

formation mechanisms would be altered by pure and simple shear. A rotated foliation pattern similar to patterns seen in the field would be consistent with dome formation prior to the major orogenic event and the associated pure or simple stress regimes. COMSOL is an elastic finite element model. Although the Harvey Cardiff system underwent ductile deformation, the elastic model approximates the instantaneous response of foliation to induced strain.

The dominant regional foliation produced by the Grenville Orogeny dips 20 degrees to the SE. The major stress field of this event would have affected preexisting structural features. Model setup is described in detail in Appendix E, with a simplified version presented here to convey the conceptual basis of the model. A circle with radius 5 km represents the dome. It has the elastic properties of granite, and is within a large block representing the mantling rocks. The surrounding rock has the average elastic properties of the mantle rock protoliths: limestone, basalt, and andesite (Elastic property values from Burger et al., 2006). I created cross-sections of expected foliations at the ground surface for probable dome formation mechanisms. Foliations are marked by ellipses, which have identical elastic properties as their host rock and are thus passive strain markers. Figure 8 shows a simplified representation of the model space with a foliation profile expected for diapirism.

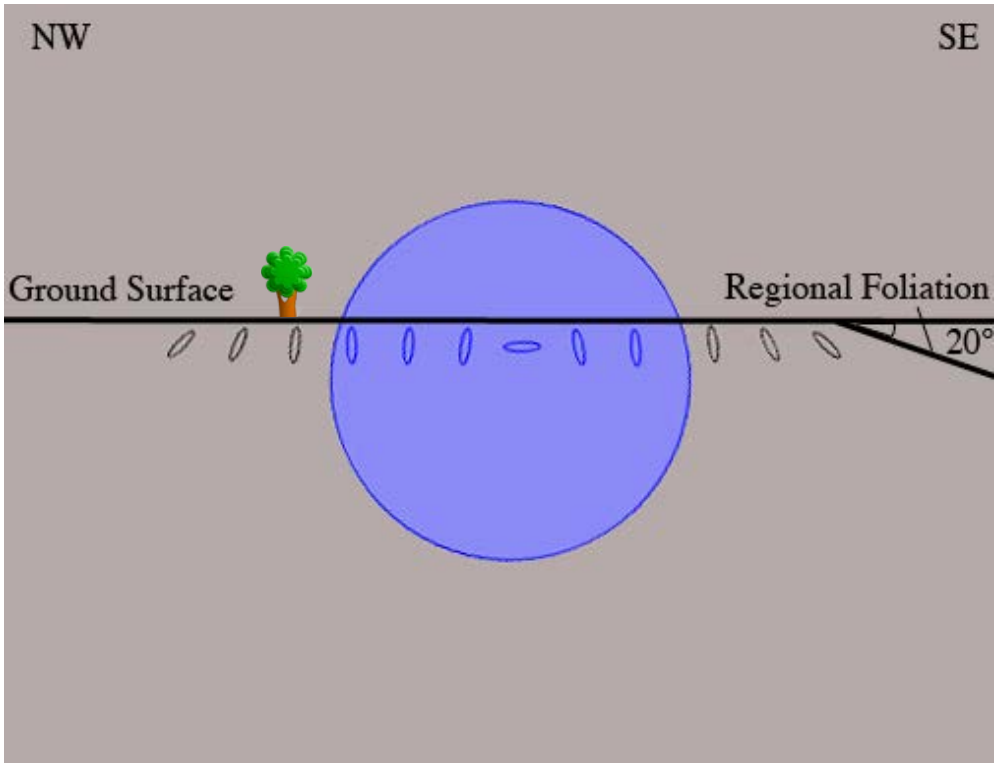

Figure 8: Schematic of COMSOL Model Setup. The circle represents the gneiss dome, and the ellipses represent foliation planes that will be distorted with applied stress. The region in purple has the elastic properties of granite, while the grey region has the average elastic properties of limestone, basalt, and andesite. Lines show the ground surface, and the dip of the regional foliation.

The direction of applied stress was determined by the regional foliation dip of 20 degrees to the southeast. In a pure shear regime, foliations form perpendicular to the maximum compressive stress. The southeast dipping foliation suggests that the maximum compressive stress during the orogeny was oriented 20 degrees clockwise of orthogonal to the ground surface. In a simple shear regime, foliations rotate to parallelism with the shear plane. If the foliation overprint was caused purely by simple shear, displacement would be along a surface rotated 20 degrees clockwise of the horizontal. Figure 9 provides an illustration of the stresses applied to the model for each strain regime.

The results of the model show how the dome and ellipse geometries change due to the applied stress. I measured the new dips of the foliation ellipses and compared them to the original dip angles to determine whether the foliations steepened or shallowed. I also assessed whether the foliations of the Cheddar Dome were steeper or shallower than the corresponding expected foliation pattern. The Cheddar Dome was selected for this comparison because of the continuous section of southeast dipping foliations running northwest-southeast. Figure 10 shows a map of the regions of foliation that I averaged using mean directions on a stereonet and compared to the model foliation patterns. If patterns of shallowing and steepening are similar in the model and the Cheddar Dome it suggests that the hypothesis of dome formation followed by rotation due to orogenic stresses is a realistic interpretation of the Cheddar Dome foliations.

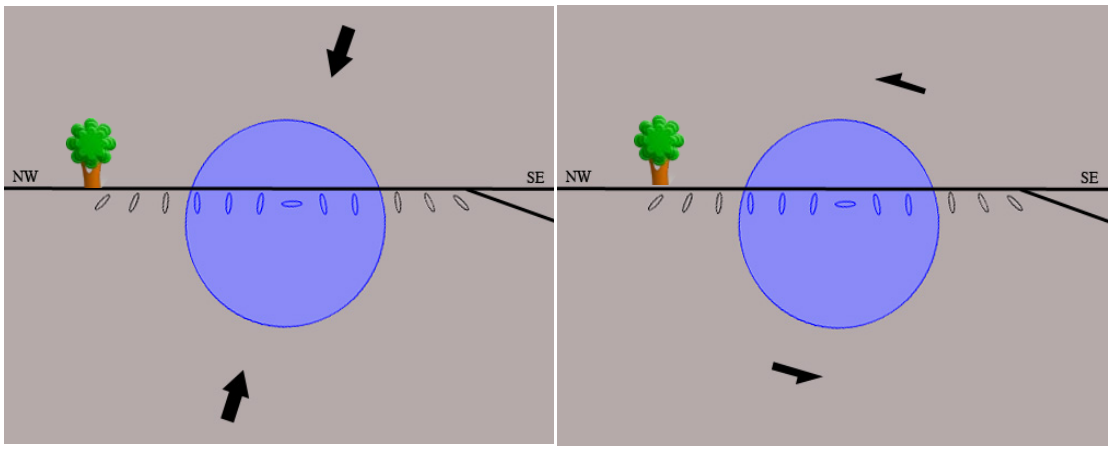

Figure 9: Strain Applied to COMSOL Models. Schematic showing directions of applied pure (Left) and simple (Right) shear to model.

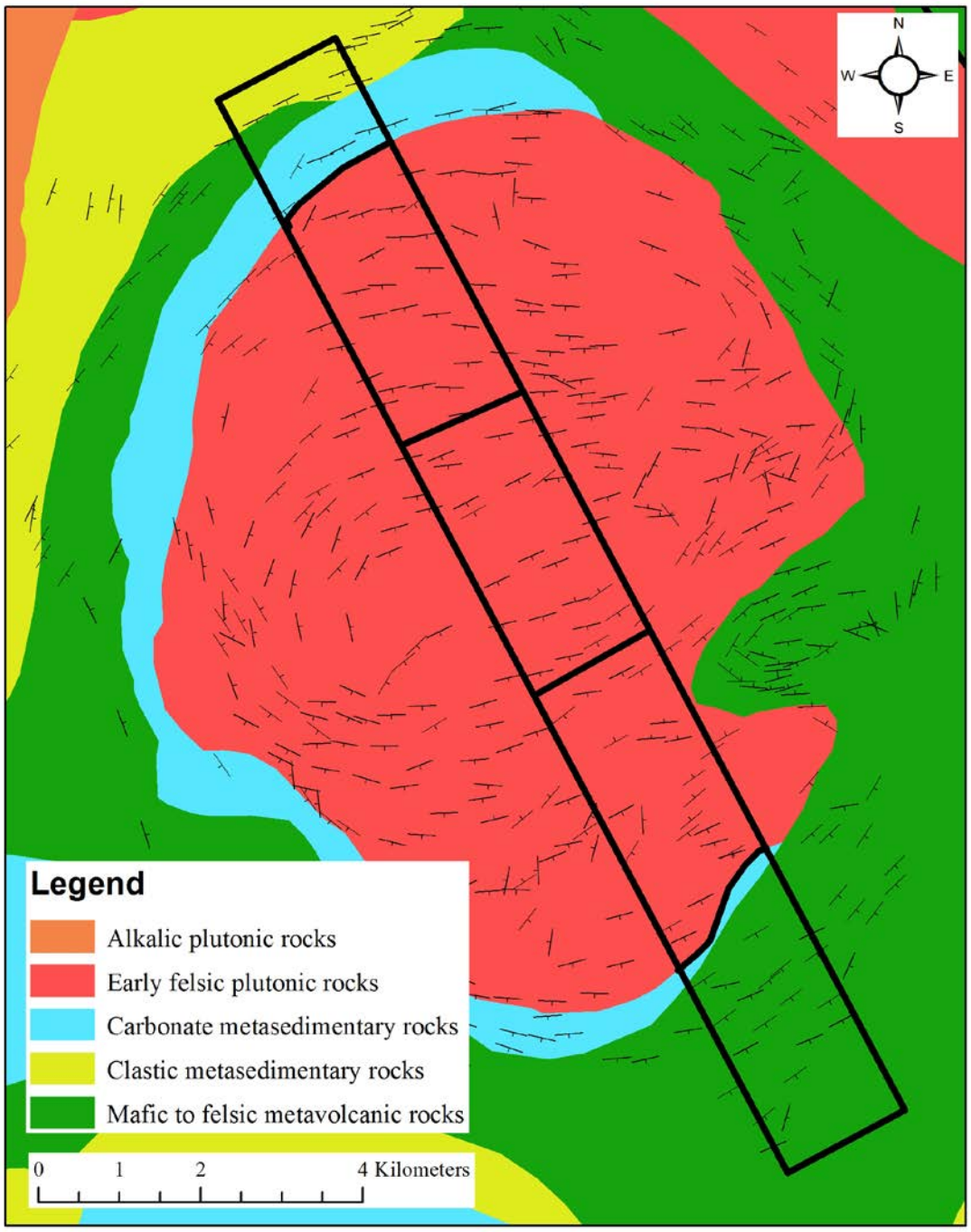

Figure 10: Foliations of the Cheddar for Comparison with COMSOL Model. Map showing the five zones of foliation that were used for comparison with the expected diapiric foliation. (*Base map from Ontario Geologic Survey).*

2.7 Dome System Analysis

Yin's classification scheme of gneiss dome systems includes two main categories, linear and non linear. As the Harvey Cardiff domes form a relatively straight line, only the linear category will be considered in this study. Two subcategories of linear arrays are presented: evenly spaced and unevenly spaced (Fig. 2). Although there is no strict differentiation between the two, type cases are cited. The Shuswap metamorphic core complex of British Columbia hosts a series of evenly spaced gneiss domes comparable in size to those of the Harvey Cardiff Domain (Teyssier and Whitney, 2002). The North Himalayan Gneiss Domes are an example of unevenly spaced domes (Hodges, 2000). In order to assess the periodicity of the Harvey Cardiff Domes and to create a quantitative basis of comparison with the two type cases, I calculated coefficients of variation for each system. This method has been applied to the study of periodicity of earthquakes (Kagan and Jackson, 1991), and is a measure of periodic variation within a system.

For each system, I calculated the distances between dome centers and found an average spacing and the standard deviation. I opened a map of each system in ArcGIS and used several spatial analysis tools to complete dome spacing measurements. I traced dome cores to produce polygons of each dome. For the Harvey Cardiff Domes, dome shape was approximated from the granitic gneiss units. The contact of the contiguous granitic units of the Anstruther and Cheddar domes and the mantle rocks were traced to create polygons. While for the Burleigh and Cardiff domes a circular shape was approximated by cutting through or including units of amphibolites and marble. I calculated the geometric centroid of each dome to a precision of three decimal places using the calculate geometry tool in ArcGIS, and drew straight lines between the centers of neighboring domes. I measured the lengths of these lines using the ArcGIS ruler and calculated the average and standard deviation for each dome system. The standard deviation divided by average gives the coefficient of variation. If the number is one, than the system is randomly assorted, if it is less than one it displays quasiperiodicity. I compared the coefficient of variation for the Harvey Cardiff domes with those of the type cases to conclude whether the gneiss domes of the Harvey Cardiff are evenly or unevenly spaced.

3. Results

This section presents results from a literature review of gneiss dome formation mechanisms as well as structural data analysis. In the first subsection, I examine each mechanism from Yin's classification scheme, along with the specific structural and metamorphic criteria that distinguish it from the others and assess the probability that each is responsible for the Harvey Cardiff Domes. The following subsections present the results of structural analysis from a variety of methods.

3.1 Possible Mechanisms of Formation

The possible mechanisms for the formation of the Cardiff and Cheddar domes can be narrowed based on associated large scale geologic features. Yin's classification scheme (see Fig. 1) groups mechanisms into two categories, domes associated with faults and domes not associated with faults (2004). These are further broken down into subcategories of different fault types for fault related, and magmatism, diapirism, and multiple folding events for fault unrelated. I assessed the likelihood that each of these subcategories produced the Harvey Cardiff Gneiss Domes by evaluating their consistency with the large scale geologic features in the region. The expected structural patterns of those that are consistent are explained and will be compared with the structures and microstructures observed in the Cardiff and Cheddar domes.

3.1.1 Fault-Related Domes

The first class of domes to be considered are the fault related domes. These include detachment related, thrust related, and strike slip shear zone related. Yin also includes ductile shear zones in her classification, however she suggests these features result from regional or local strain fields, rather than being the initiators of dome formation. Because of this, I did not review them as a possible mechanism for the formation of the Harvey Cardiff Domes. As follows from the name, each of these mechanisms requires a fault or shear zone large enough to produce gneiss domes approximately 10 km in diameter. Due to the size, such features would most likely be apparent in maps and recognized in the literature of the area.

Detachment Faults:

Mechanism

Detachment faults can produce gneiss dome structures when corrugated. As the low angle fault accommodates extension, it can be synchronously warped due to isostatic rebound in later stages of its development (e.g. Wernicke and Axen 1988) or extension orthogonal contraction (e.g. Martinez-Martinez et al., 2002). A horizontal erosion surface intersecting the warped fault would produce domal patterns. Figure 1 shows two end member cases of detachment fault associated domes, these reflect hanging wall response to different amounts of crustal thinning.

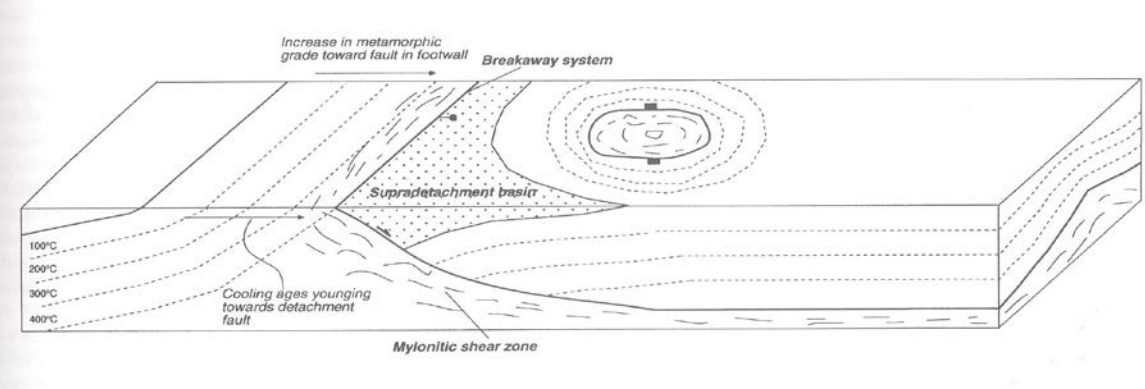

Figure 11: Features of a Detachment Fault Related Gneiss Dome. Schematic of gneiss dome formed by extensional detachment faulting. Note the presence of a supradetachment basin, an increase in footwall metamorpic grade towards the fault, and a decrease in cooling ages approaching detachment fault. *(From Yin, 2004).*

Criteria

If domes are formed by detachment faulting, they are associated with the important features of this process, namely an identified detachment fault and a supradetachment basin where sediments fill in the basin created by normal listric faulting. In the footwall metamorphic grade increases and cooling age decreases in the direction of the detachment fault. Recognition of a ramp cutting metamorphic grades is key in distinguishing detachment fault related from thrust fault related gneiss domes.

Application to Harvey Cardiff Domes

Because the Grenville has not been associated with deep rooted detachment faulting, and due to the lack of an evident fault or supradetachment basin, this explanation can be reasonably excluded for the formation of the Harvey Cardiff domes.

Thrust Faults:

Mechanism

Two distinct processes have been identified as mechanisms for gneiss dome creation associated with thrust faulting. Both require bounding thrust faults that excavate deep crustal rocks and form the core. In the first instance, a series of thrust faults coalesce to expose part of the deep crust. This is entitled a thrust duplex, and is cited as the process leading to the development of the Kangmar Dome in Tibet (Makovsky et al., 1999). The second also has a passive roof fault that keeps the rocks in the subsurface (Fig. 12).

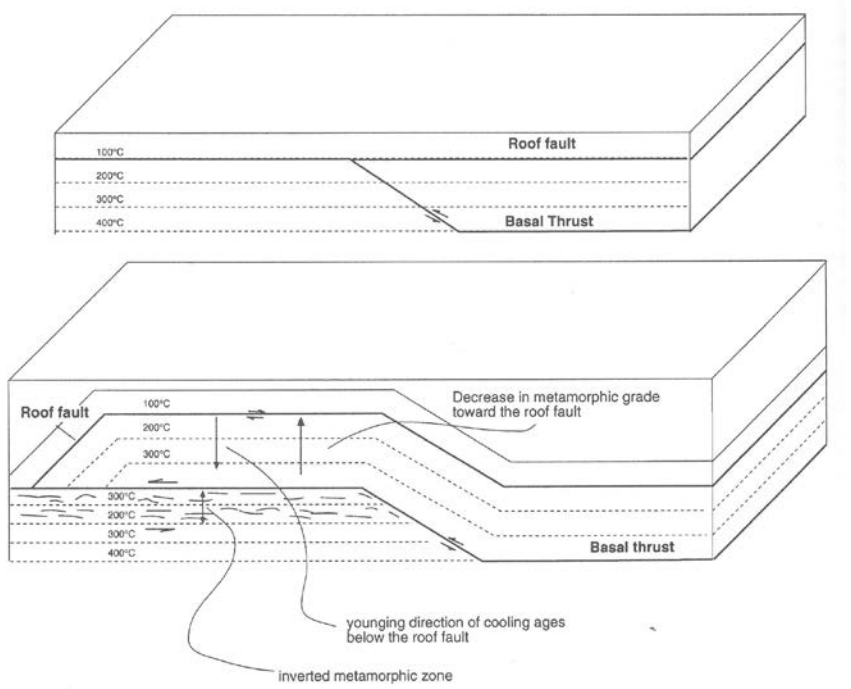

Figure 12: Features of a Thrust Fault Related Gneiss Dome. Schematic of gneiss dome formation assocaited with passive roof thrusting. Note that metamorphic grade decreases toward the thrust and footwall cooling ages young away from the roof fault. *(From Yin, 2004).*

Criteria

A horizontal section of the faulted area will expose a dome of higher grade rock surrounded by the basal thrust. These domes can be distinguished from detachment-related gneiss domes based on patterns of metamorphic grade. Isograds in this situation display a flat-over-flat geometry where the fault ramp does not cut across the metamorphic gradient. Metamorphic grades decrease towards the passive-roof thrust, and cooling ages young away from the it.

Application to Harvey Cardiff Domes

No bounding thrust faults along the core-mantle contact are observed in the Harvey Cardiff Domes. Thus, a thrusting origin is unlikely for this dome set.

Strike Slip Shear Zone:

Mechanism

Gneiss domes can also develop as broad folds in a strike slip shear zone. This mechanism has been proposed for a line of domes along the Raikot fault in northern Pakistan. In this setting, broad dextral shearing in a transpressive region is interpreted to have caused a crustal scale folding system (Pêcher & Le Fort, 1999).

Criteria

This mechanism requires that the domes exist within a broad strike slip zone several tens of kilometers wide.

Application to Harvey Cardiff Domes

The Harvey Cardiff domain is characterized by thrusting, not strike-slip motion. The domes are not within a broad strike slip zone, and therefore this mechanism can be excluded

3.1.2 Fault-Unrelated Domes

The second category of gneiss domes are those unrelated to faults. This includes domes formed by diapirism resulting from magmatism or contrasts in mechanical rock properties, and domes formed by superposition of multiple folding events. The former is not associated with any regional geologic features, and thus is a feasible mechanism for formation of the Harvey Cardiff domes. Polyphase folding is a widely recognized mechanism for producing gneiss domes. Folding patterns on a regional scale should indicate whether stress and strain patterns produced folding events favoring dome creationg.

Multiple Folding Events:

Mechanism

In order to create domes from multiple folding events, the axial planes must be out of alignment with one another. The simplest case to consider is one with two orthogonal folding events, producing a doubly plunging anticline (Fig. 13). If the older beds forming the center of the anticline are composed of gneisses, this feature would be consistent with the definition of a gneiss dome. There is no technical distinction between a gneiss cored doubly plunging anticline and a gneiss dome, although gneiss domes require a degree of radial symmetry and thus must be circular to oval (Van Staal & Williams, 1983). The degree to which axial planes can diverge from orthogonal and still produce a gneiss dome is also not established, and depends on fold interaction within a three dimensional space.

Criteria

In order to produce gneiss domes from multiple folding events, the axial planes must have varying strikes. Below are two computer generated examples of polyphase folding events (created using Visible Geology Beta, available at http://app.visiblegeology.com/profile.html). The first is simple orthogonal folding creating doubly plunging anticlines. The domal geometry created is evident in map view. The second set shows two folding events with axial planes striking 20 degrees from one

another. This produces an elongate ellipse in map view, and less clearly resembles a dome shape. Adding variations in dip and hinge plunge further complicates the possible folding patterns. However, if the axial planes are close to parallelism it is unlikely that doming will occur (Van der Pluijm & Marshak, 2004).

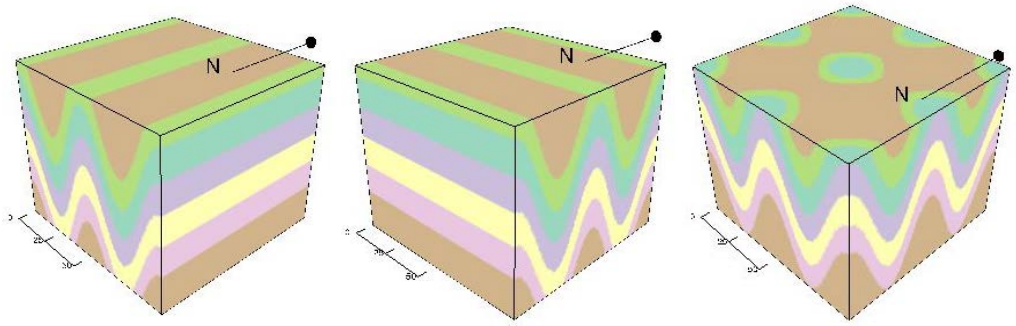

Figure 13: Superposition of Orthogonal Folding Events. The first folding event (*Left)* has axial planes striking north-south. The axial planes of the second event (*Middle*) strike east-west. The polyphase result *(Right)* produces a doubly plunging anticline, with a dome structure evident in map view.

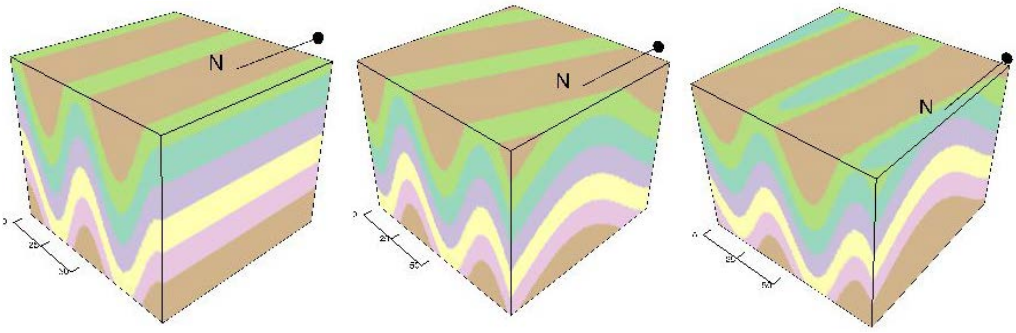

Figure 14: Superposition of Non-Orthogonal Folding Events. The first folding event (*Left)* has axial planes striking north-south. The axial planes of the second event *(Middle)* strike N20E. The polyphase result (*Right*) produces a visible anticline in map view that has an elongate oval geometry.

Application to Harvey Cardiff Domes

Evidence of at least three generations of folding is documented in an area 30 km west of the domes (Divi & Fyson, 1973). The axial plane of the first event is parallel to bedding, and has no folding effect. The axial planes of the second and third events both strike northeast, although F_2 dips moderately to the southeast while F_3 is upright and has a shallowly plunging hinge. Figure 15 shows the result of the combination of folding events in the Harvey Cardiff. No dome structures appear in map view, and therefore it is unlikely that these events caused the formation of the Harvey Cardiff Domes.

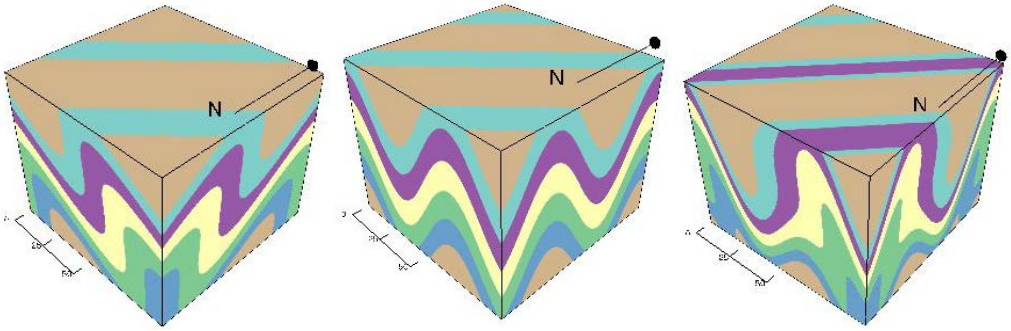

Figure 15: Polyphase Folding of the Harvey Cardiff. The first event is not pictured here because its axial plane was parallel to bedding. F_2 *(Left)* strikes N45E and dips 60 degrees to the southeast. F_3 *(Middle)* also strikes N45E but has a dip of 0 and its hinge plunges 10 degrees to the northeast. The polyphase result *(Right)* does not display dome structures.

Diapirism:

Mechanism

Diapirism is the mechanism of formation cited in the earliest studies of gneiss domes, and has been ascribed to domes worldwide (e.g. Brun et al., 1981; Hippertt, 1994; Bouhallier et al., 1995). Diapirism describes the upward travel of material through surrounding bedrock due to instabilities produced by contrasts in mechanical rock properties. Such movement can be triggered by a variety of factors including density inversion and instabilities due to viscosity contrasts (Yin, 2004). Density inversions cause the lower layer to bow-up and rise by solid state flow through the crust. This upward movement is aided by decompression melting and rheologic weakening of the host rock due to heat flux from the diapir. The density inversion may be initiated by magmatism, or magmatism can result from decompression melting of the rising diapir. This decompression is often recorded in migmatites that are found in many gneiss dome cores. (Amato et al. 1994).

Density inversions can also be created during regional metamorphism that exposes layered rocks to high pressure and temperature conditions. During burial and heating, metasedimentary rocks may become as dense as, or denser than granitic composition basement rocks. For example, garnet and biotite bearing metapelites have a density of between 2.7 and 2.9 g/cm^3, while biotite-plagioclase-quartz gneisses have a density of 2.5 to 2.7 g/cm^3 (Teyssier & Whitney, 2002). Decompression allows the diapirs to continue to rise through the crust at near constant temperatures. A similar process can occur due to instabilities produced by vertical viscosity contrasts in the rock. Lower viscosity material underlying higher viscosity rock will rise if placed under

contraction, and continue to rise due to decompression melting and rheologic weakening of the surrounding crust (Yin, 2004).

Criteria

Analog centrifuge models have been used to examine structural patterns of diapiric domes in cross section. Dixon (1975) performed a series of experiments using layers of putty with varying specific gravities and viscosities that produced diapiric features when centrifuged. The dome core is represented by a low specific gravity layer (1.40), and is overlain by a layer with a specific gravity of 1.56. Putty layers were cut into horizontal and vertical laminations that form undeformed square elements when superimposed. Deformation was recorded in the shape change of these elements from the original square. Models were subjected to different lengths of centrifuging to produce different stages of domal development. The models that could be evaluated for strain formed cylindrical ridges, rather than spherical diapirs. Figure 16 shows analogue models for both mid and late stage dome development. Initially flat layers bow-up and develop a domal structure. The shape and structural patterns within diapiric domes vary with stage of development and cross section depth, and can be applied to natural domes.

In these experiments, as the dome develops**,** its top broadens after reaching the free surface, while the neck becomes skinnier and more pronounced. Figure 17 shows the maximum elongation directions at 200 points in the dome core and mantle for domes in both stages of development. Within the dome core, maximum elongation strain can be used as a proxy for lineation direction, and the formerly horizontal layers demonstrate foliation patterns. The overburden layers are likely to deform along any previously defined planar features, such as bedding planes. In this model the original mantle bedding planes were horizontal before gneiss dome emplacement. Lineation consistent with stretching direction will develop on these planes. Figure 17 also illustrates the depths of cross sections described in the following paragraphs. It is worth noting that foliation patterns at a particular depth are consistent across both the core and mantle.

The cross section of the less developed dome has a roughly semicircular dome top and shallowly sloping flanks. The first cross section considered is through the upper portion of this dome at line A of Figure 17. At the center of the dome foliation is horizontal. Moving laterally outwards in the dome the core foliation shifts to dipping moderately away from the dome. Lineations are also horizontal in the center of the dome and steepen away from the dome center. A deeper section across the lower portion of the dome is pictured as Line B in Figure 17. At this depth foliations in the center of the dome

are vertical and gradually shallow, dipping away from the dome. Lineations are vertical in the dome center, transitioning first to plunging towards the dome center, and then away. Sense of shear is top outwards in both the core and mantle of all depths.

In a more developed dome the upper portion of the diaper bows outwards and the flanks move to, or past, vertical. Line C of Figure 17 shows a transect through the upper portion of the diapir. Foliations in both the core and mantle are close to horizontal, but dip slightly towards the dome center. Lineation in the core transitions from plunging towards the center to plunging away. In the mantle, lineation plunges along the dip of foliation. The deeper transect intersects the dome at line D of Figure 17. Foliations in the core and inner mantle dip steeply towards the dome center. At a distance from the dome mantle foliation shallows and eventually dips back towards the dome center. This pattern is mimicked by lineation. Again, sense of shear is top outwards in all cases.

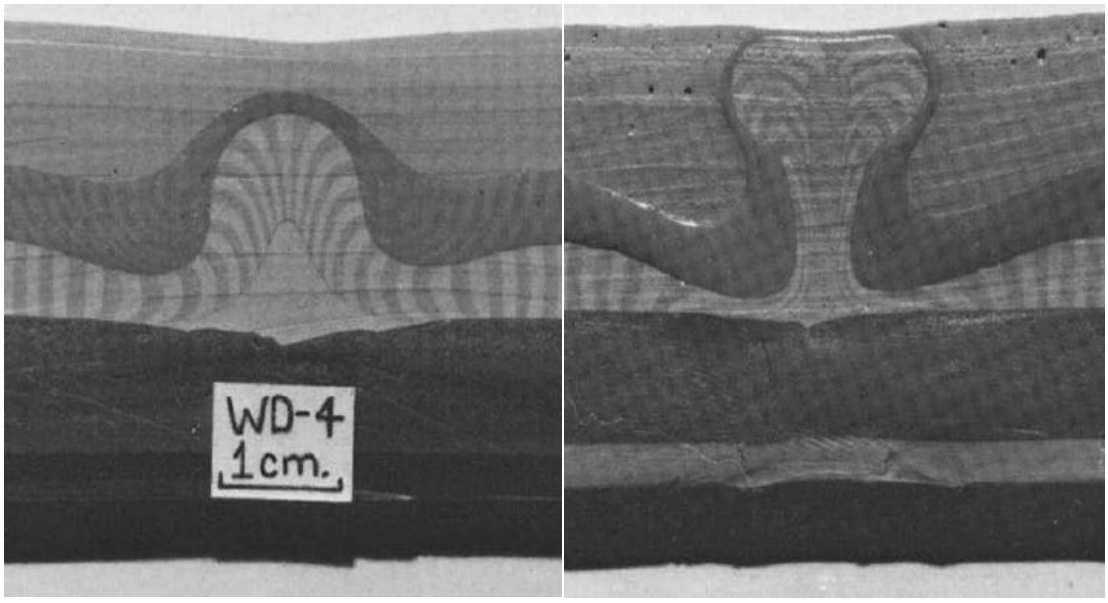

Figure 16: Analogue Models of Diaprisim. Analogue models of dome development for less developed (*left*) and more developed (*right*) gneiss domes. The striping in the two middle layers are the vertical laminations that were superimposed upon an identical sections from the same block that had horizontal laminations and used to track strain. The lighter striped layer is the less dense core layer, and the darker layer covering it is more dense and represents the mantle (*From Dixon, 1975*).

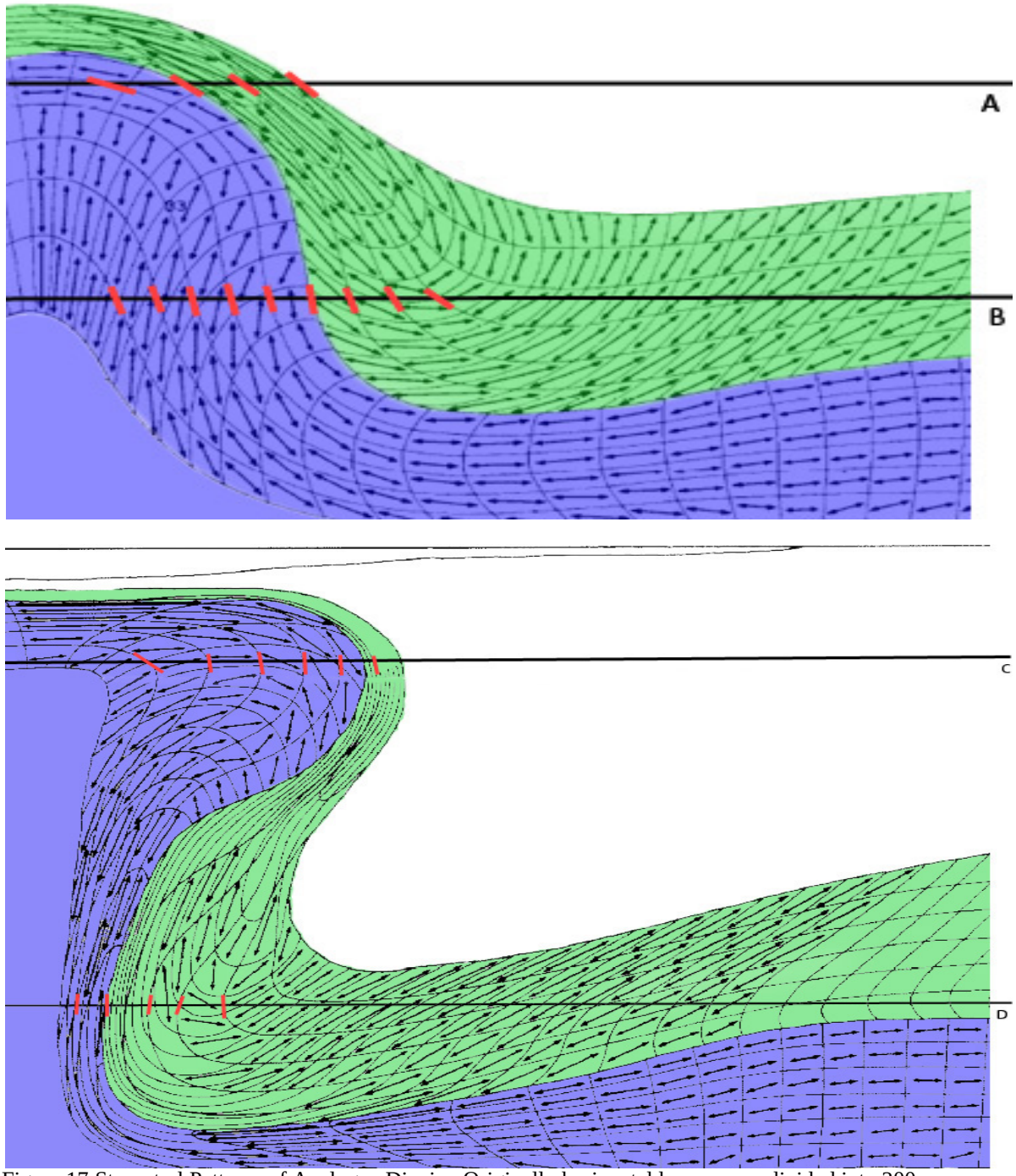

Figure 17:Sturcutral Patterns of Analogue Diapirs. Originally horizontal layers were divided into 200 segments and then drawn after deformation. The formerly horizontal lines represent expected foliation directions in both the core and mantle. The double arrows represent maximum elongation directions, which act as a proxy for stretching lineation direction within the dome. In the mantle, strain is expected to be accommodated along original bedding layers, and lineations develop within that plane. The figure represents two stages of diapir development: less developed *(Top)* and well developed *(Bottom)*. Lettered lines show cross sections described in the text. Red lines along the cross section highlight the dip of foliation along the transect. (*Modified from Dixon, 1975)*.

Application to Harvey Cardiff Domes

Diapirism is not associated with an large scale geologic features, and is the most likely explanation for the Harvey Cardiff Domes after the elimination of the mechanisms discussed above. Slight adaptations were made to the interpretation of the cross sections here to account for radial formation rather than cylindrical dome formation. The formation of the complex of Grenvillian gneiss domes in northern Québec has been attributed to this mechanism by a structural study focused on the principle stretching axes of conjugate flanking shear bands (Gervais et al., 2004). Thus, it is reasonable to consider diapirism as a mechanism for the Harvey Cardiff Domes.

3.3 Cardiff Dome Structural Analysis

The most prominent foliation pattern in the Cardiff Dome strikes east-northeast and dips to the south. This is consistent with the dominant region foliation pattern discussed above, and was removed from most data sets to highlight other structural patterns. Figure 18 shows the foliation data subdivided into seven regions. Starting at the north, twenty-four out of the twenty-six foliation measurements in region I fall within thirty degrees of the dominant foliation. This stereonet is the only one in this figure that includes measurements within this range. They dip towards the dome center in both the core and the marble of the mantle. In region II, foliation strikes predominantly east-west mostly dipping to the south. However, there is a significant portion of foliations in the core and mantle that dip the opposite way, towards the north. The foliation in region III varies greatly with dip. The northernmost portion of this region is strongly affected by the dominant foliation, however because this was excluded for this analysis it does not appear in the stereonet. Other foliations dip north or northeast away from the dome center. Region IV displays two maxima that reflect the curving of foliations about the dome center. Both dip to the southeast away from the dome. Region V foliations dip to the southwest away from the core. Region VI shows a wide variety orientations, dipping mainly away from the core in the inner radius of the dome, and away at the outer. Region VII foliations dip shallowly to the southeast towards the dome in both the core and mantle.

Although it is difficult to distinguish the core and mantle in the Cardiff Dome, there is no evident distinction between their foliation patterns. Foliation in the northeast, south, and a portion of the west dip away from the dome, while those in the north and northwest more consistently dip towards the dome core. Lineation within Cardiff Dome plunges shallowly to moderately to the southeast (Fig. 13).

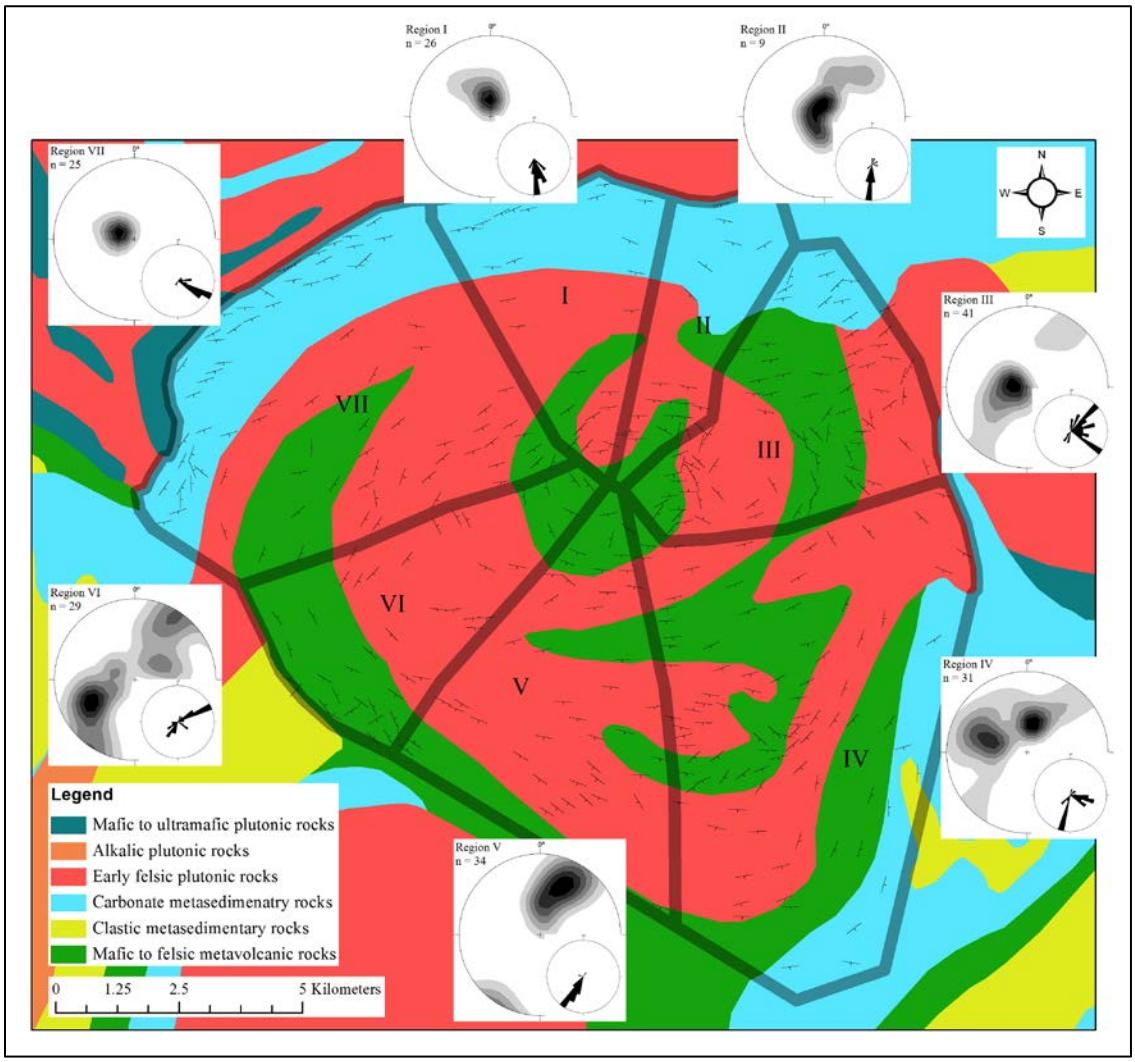

Figure 18: Foliation Orientations of the Cardiff Dome. Foliation orientations in the seven regions of the Cardiff Dome. Stereonets show contoured plots of poles to foliation planes within each region. Rose diagrams plot dip direction. Excepting region I, all plots exclude foliations striking within 30 degrees of the regional maxima (those with strikes of 40-100). (*Base map from Ontario Geologic Survey).*

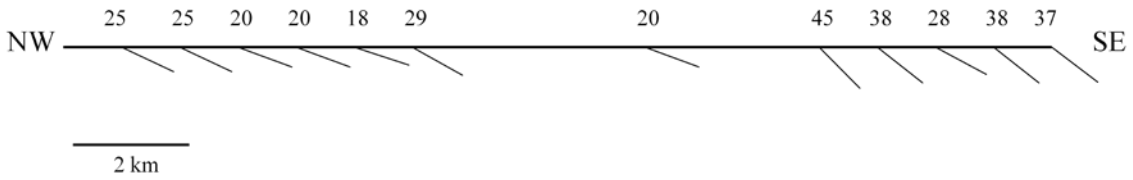

Figure 19: Cross Section of Cardiff Dome Perpendicular to Dominant Foliation. This cross section is 17 km long, and shows average foliation dips for every 1 km. In regions with no dip information there were no foliations dipping in the orientation of the cross section.

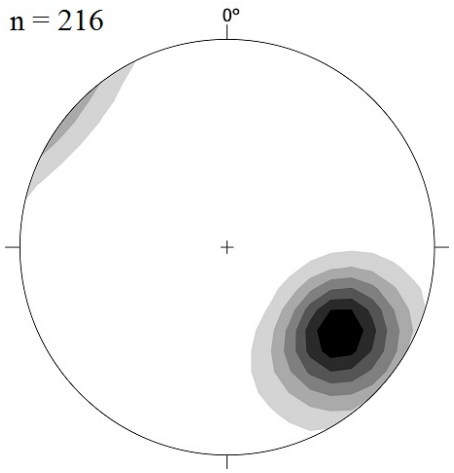

Figure 20: Lineations of the Cardiff Dome. Contoured plot of all lineations in the Cardiff Dome core and mantle.

3.2 Cheddar Dome Structural Analysis

The foliation patterns in the Cheddar Dome resemble those of the Cardiff Dome to the North. The Cheddar Dome also shows the dominant regional foliation orientation striking east-northeast and dipping moderately to the southeast. lineation shows a wider range of moderate to shallow plunges to both the east and west (Fig. 12).

Figure 21 presents the foliation data subdivided into seven regions. In some cases there is a significant difference in dip within these data sets, reflected in separate maxima on the contour plots. The central region (region I) shows very strong concurrence with the overall foliation trend, with foliations dipping moderately to the south-southeast. In Figure 21, the region I stereonet is the only stereonet to include foliations with dip directions between 130-190 degrees. Moving clockwise around the dome from the top center, region II, in the northeast, has two maxima. Foliations associated with the strongest maximum dip steeply to the northeast, away from the dome core. Sub-horizontal foliations make up the much smaller second maximum. Region III contains foliations dipping primarily away from the dome to the northeast. The two maxima of region IV demonstrate the curvature of the foliation around the domal contact, with foliations striking east-northeast, but dipping moderately to the north and south. Region V is the southeast side of the dome and most foliation here dips moderately to the northwest and towards the dome core. A second maximum is composed of mantle foliations of similar strike that dip shallowly away from the center of the dome. The west side of the dome shows two distinct zones of foliation. Region VI, on the southwest side of the dome, shows a foliation dipping moderately to the southwest, away from the dome. Region VII, on the west side of the dome, shows two

maxima, with foliation dipping steeply to the east. Stretching and c-axis orientation lineations in the region trend east west. In the mantle, lineation plunges moderately to the east (Fig. 23).

In summary, foliations dip both towards and away from the dome center in both the core and mantle. Some regions show two maxima for foliation orientation, while others show a single maximum. Foliations in the northeast, east, and south (regions II, III, IV, and VI) more consistently show dips away from the dome core. Foliations in the north and northwest dip toward the core along with region V, in the southeast.

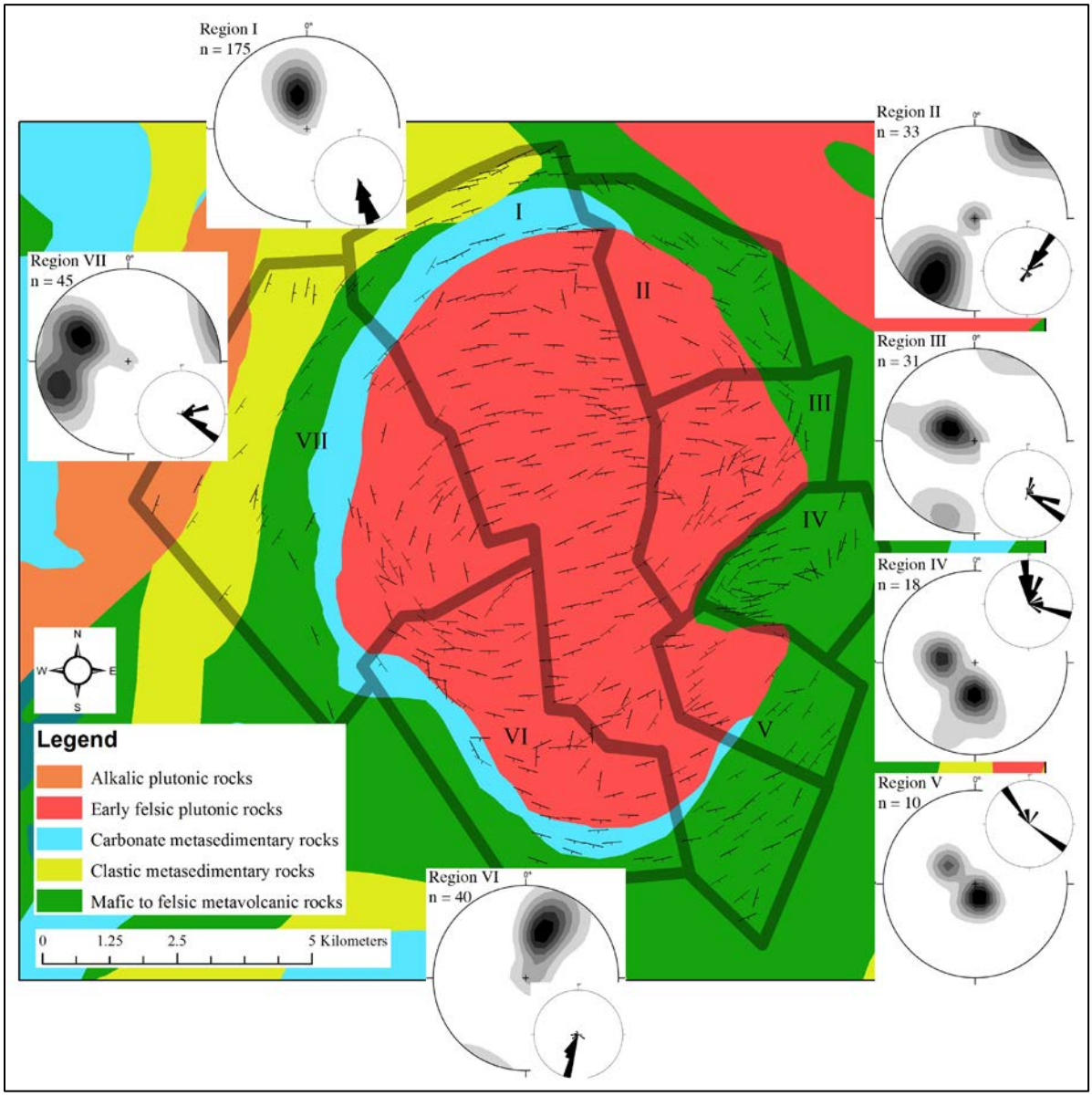

Figure 21: Foliation Orientations of the Cheddar Dome. Stereonets show contoured plots of poles to foliation planes within each region. Rose diagrams show dip direction. Excepting region I, all plots exclude foliations with strikes of 40-100. (*Base map from Ontario Geologic Survey).*

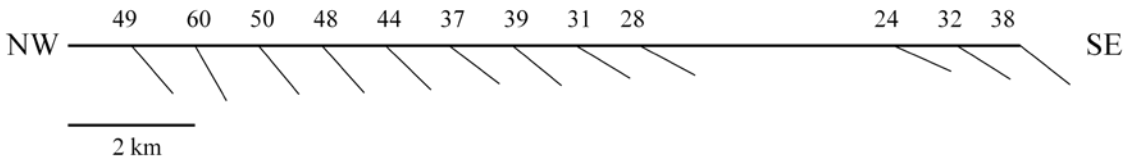

Figure 22: Cross Section of Cheddar Dome Perpendicular to Dominant Foliation. This cross section is 15 km long, and shows average foliation dips for every 1 km. In regions with no dip information there were no foliations dipping in the orientation of the cross section.

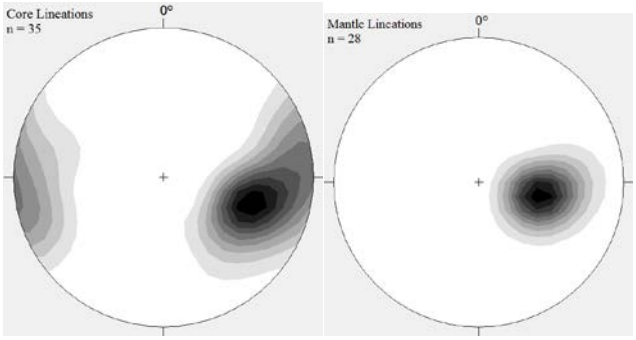

Figure 23: Lineations of the Cheddar Dome. Contoured stereonets of core *(Left)* and mantle *(Right)* lineations of the Cheddar Dome.

3.4 COMSOL Analysis

Figure 24 shows the COMSOL results of both pure and simple shear models. The translation of the resultant dome is due to model setup and does not affect the foliation rotations. The original dip of each of the twelve foliation ellipses is presented in Table 1 below along with the resultant dips after pure and simple shear were applied. Also included in the table are the average dips of comparable regions in the Cheddar Dome. Foliations in the northwest steepened (represented in green) or overturned (in green and bold), while those in the southeast shallowed (in blue), excluding element 12 which steepened slightly. This pattern is consistent with the foliations of the Cheddar Dome, which are overturned from the expected in the northwest and shallower than expected in the southeast.

	Foliation Dip											
Model	1	2	3	4	5	6	7	8	9	10	11	12
Original Dip	45N	65N	83N	90N	85N	80N	0	80S	87S	83S	65S	45S
Pure Shear	47N	72N	**85S**	**75S**	**80S**	85N	0	58S	72S	63S	53S	47S
Simple Shear	55N	74N	**86S**	**81S**	**86S**	89N	0	74S	79S	75S	61S	46S
Field	**50S**			**49S**		35S		24S		36S		

Table 1: COMSOL Results. Each numbered column represents one foliation ellipse. Red numbers are foliations in the mantle, and black are in the core. Green dips indicate that the resultant foliation from the models or field data was steeper than that of the normal section of a diapir. Bold green dips indicate that the foliation has overturned. Blue dips indicate that the foliations have shallowed.

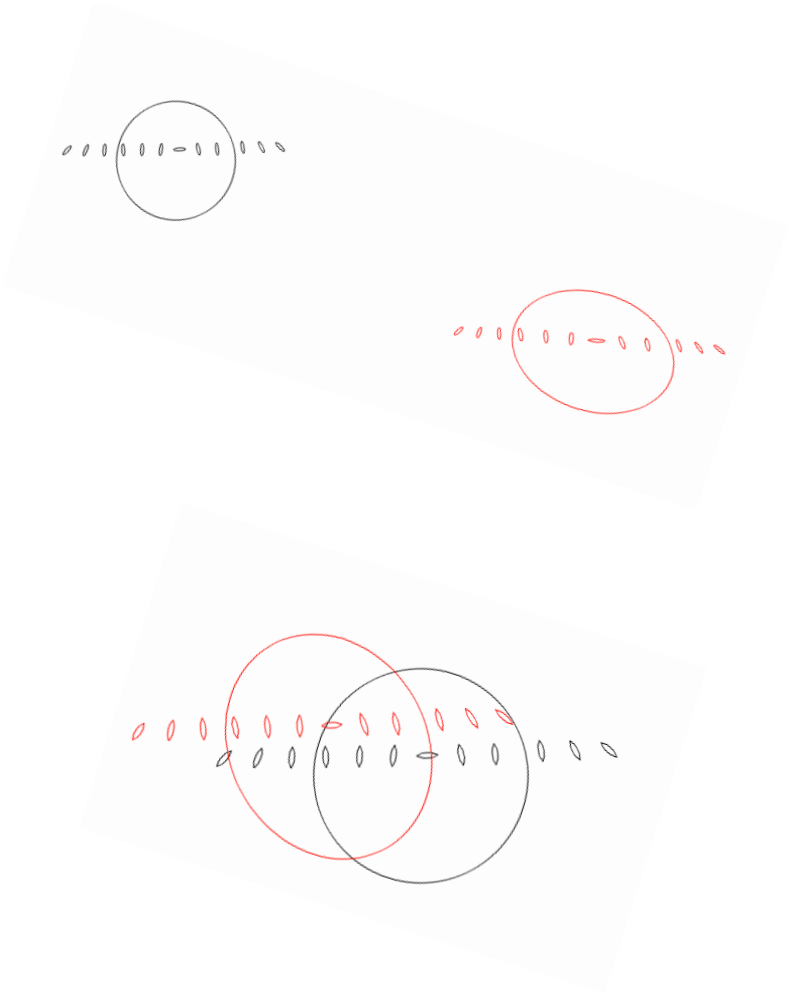

Figure 24: COMSOL Results. Results of pure shear (*Top*) and simple shear (*Bottom*). Original dome and foliation ellipses are in black, while resultant ones are in red.

3.4 Thin Section Analysis

I analyzed thin sections for composition, fabric analysis, and sense of shear indicators. Appendix C shows photomicrographs of all thin sections. The amphibolite samples were predominantly quartz and feldspar, with varying ratios of plagioclase to orthoclase. Some contained up to 40% clinopyroxene. Foliations were defined by amphibole, biotite, or a mixture of the two. Some magnetite and other opaques were present. The granitic gneisses were composed of primarily quartz, plagioclase, and perthitic orthoclase. Two samples had clear foliation defined by hornblende and biotite. The marble contained calcite and diopside grains. The biotite schist contained quartz, small amounts of plagioclase, and a biotite foliations.

Although amphibolites in the dome's mantle show strong foliation and lineation defined by compositional banding and orientation of amphibole and biotite grains, they lack a clear sense of

shear at the scale of hand samples or thin sections. Instead, most of these rocks display triple junction grain boundaries (Fig. 25) and appear to have statically annealed.

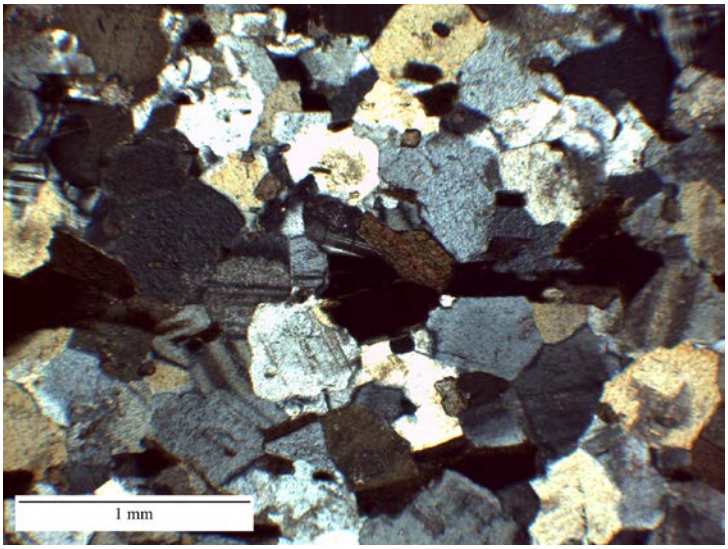

Figure 25: Triple Junction Grain Boundaries in Thin Section. A representative thin section that shows triple junction grain boundaries, indicative of static annealing.

3.5 Dome System Analysis

The calculated centroids of each dome and measured spacing values are displayed in Figure 26. Values for the measured spacing, average, standard deviation, and coefficient of variation are displayed in Table 2 below. The coefficient of variation for the Harvey Cardiff Domes is 0.26, making them a quasiperiodic grouping. The value for the type case for the evenly spaced domes of the Shuswap complex in British Columia is 0.24, and the value for the type case of unevenly spaced North Himalaya Gneiss Domes is 0.7 (see Appendix E for calculations). Although both systems have coefficients of variation less than one, there is a clear distinction in numerical value between evenly and unevenly spaced. The Harvey Cardiff Dome system falls in the range of the evenly spaced domes.

Distance from Burleigh to Anstruther	18.8 km
Distance from Anstruther to Cheddar	16.8 km
Distance from Cheddar to Cardiff	11.0 km
Average Spacing	15.5 km
Standard Deviation	4.0
Coefficient of Variation	0.26

Table 2: Dome Spacing Calculations. Measurements of dome spacing and calculated average standard deviation and coefficient of variation.

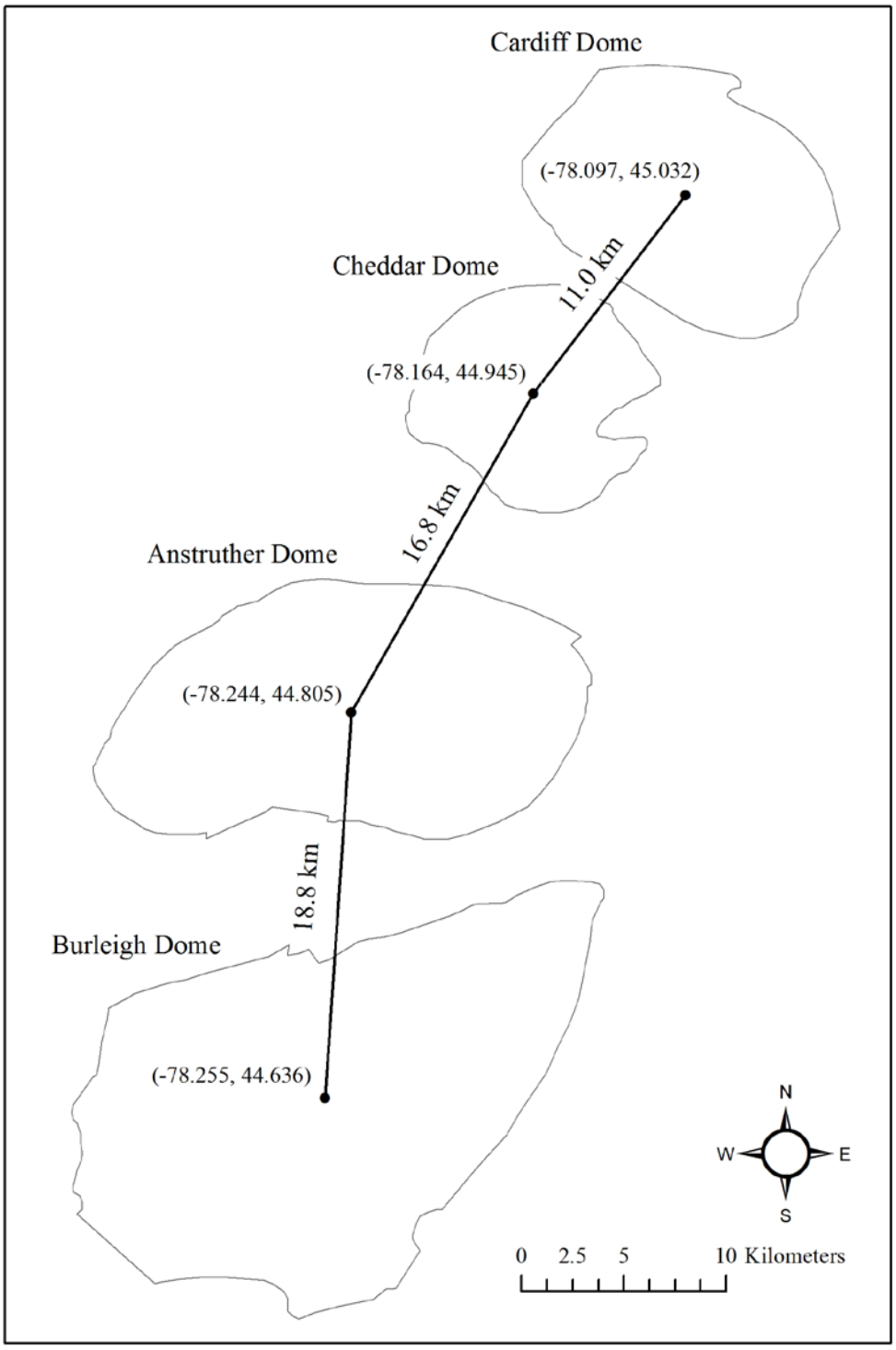

Figure 26: Spacing of Harvey Cardiff Domes. Outlines of domes with latitude and longitude of calculated centroids and calculated distances between them.

4. Discussion

4.1 Dome Formation

Structural analysis of individual domes as well as the periodicity of the gneiss dome complex suggests that the domes of the Harvey Cardiff Domain formed by diapirism.

4.1.1 Cardiff Structures

The Cardiff Dome exhibits a mixture of outward and inward dipping foliations that are not radial symmetric about the dome as would be expected in the ideal diapir. Foliations on the northern side of the dome (regions I, II, IV, and VII) are consistent with a deep slice through a well-developed diapir (slice D in Fig. 17), where foliations dip towards the dome in both the core and mantle. The southern portion (regions III through VI) is more consistent with a shallow slice (slice C in Fig. 17) where foliations dip outward in both regions. The current exposure of the Cardiff Dome represents an apparent non-horizontal slice through a diapir, exposing a deeper section to the north and a shallower one to the south. However, the foliation patterns clearly relate to the typical southeast dip of foliation in the Central Metasedimentary Belt boundary thrust zone (CMBbtz) just to the west of the Harvey-Cardiff Arch (Hanmer 1988; Hanmer and McEachern 1992). This indicates that the major orogeny which formed these foliations elsewhere in the region interacted with purely the diapiric foliation. The Cardiff dome also shows a lineation trend predominately to the southeast, consistent with lineations widely reported for the CMBbtz.

4.1.2 Cheddar Structures

The Cheddar Dome shows foliation patterns very similar to those of the Cardiff Dome. Foliations are not radial symmetric about the dome, but instead dip towards the dome to the north and away in the south. The same scenario of a non-horizontal slice through the diapir exposing a deeper section to the north and a shallower one to the south is also consistent with the Cheddar Dome. Again, foliation patterns are dominated by the southeast dipping trend, and reflect the patterns seen in the CMBbtz. The Cheddar Dome does, however, show a lineation that is distinct. The shallowly-dipping east-trending lineation differs from the southeast-trending lineation widely reported for the CMBbtz.

4.1.3 Gneiss Dome System

Domes of the Harvey Cardiff Domain are evenly spaced. This classification is not diagnostic of any particular mechanism. Domes caused by buckling and rock property contrasts all tend to form evenly spaced domes in laterally homogeneous matter. Therefore, these results are consistent with the hypothesis of diapirism. However, it is also possible for the other mechanisms to produce evenly spaced domes. Also it must be remembered that the environments in which

domes form are not equivalent to those in the laboratory, and no evidence exists that the mechanisms mentioned above must form evenly spaced domes (Yin, 2004).

4.2 Possibility of Overprinting

Although the foliation pattern seen in the Cardiff and Cheddar Domes is consistent with a nonhorizontal slice through a diapir, this seems physically unlikely and is not discussed in gneiss dome literature to date. A more feasible solution is that foliations related to the diapir were affected by orogenic stress fields during the orogeny.

The prominent south-southeast dipping foliation seen in the Cardiff and Cheddar Domes most likely resulted from the large-scale, regional strain field of the orogenic collision. The maximum presented in Figure 7 is within thirty degrees of the orientation of the orogeny axis in Ontario (Tollo et al., 2004). This overprinting could have occurred in concurrence with, or after gneiss dome formation, as the regional strain field will generally be much larger than any local strain field associated with dome formation (Yin, 2004).

The COMSOL modeling results demonstrate that a Harvey Cardiff Dome that began as a diapir with the expected radially symmetric foliation pattern would appear as a nonhoizontal slice when subjected to either pure or simple shear. Foliations rotated to steepen and overturn in the northwest, mimicking a deeper slice through a diapir; while they shallowed in the southeast, mimicking a shallower slice. These results show that it is structurally possible to create an apparent nonhorizontal slice by subjecting a normal diapiric foliation pattern to the strain of a major orogenic event. However, this does not exclude the possibility that dome formation was synorogenic.

Lineation in the Cardiff Dome appears to have been overprinted by the main orogenic event, however lineations within and outside the Cheddar Dome indicate stretching in the east-west direction. Looking at infinitesimal strain, both stretching lineations and foliations tend to form perpendicular to the maximum compressive stress. If the region were undergoing pure shear from the compression of the orogeny, the maximum compressive stress remains constant, and the foliations and lineations should be aligned with the trend of the orogen. Thus, foliations should be striking at 040, approximately the same trend as mineral lineations. If instead the system were formed under simple shear, the foliation and lineation direction would rotate with progressive amounts of strain. In the case of the Cheddar and Cardiff Domes, the orientation of the orogen is more northerly than the attitude of foliation and lineation. This suggests that there was a component of simple shear present during the orogeny.

4.3 Post Metamorphic Conditions

The lack of shear sense indicators and the presence of triple junction grain boundaries suggests that the dome rocks were retained at high temperatures after deformation. Through the processes of static recrystallization and grain boundary area reduction, the internal free energy of the system is reduced and deformed grain boundaries straighten (Passchier & Trouw, 2005). The Harvey Cardiff Domes were emplaced into the mid to lower levels of the orogeny into crust that was most likely raised above the geothermal gradient due to the heat of continental collision (Cosca et al., 1995). Thus it is probable that much textural evidence was lost during static recrystallization late in the orogenic cycle.

5. Conclusion

The domes of the Harvey Cardiff Domain have clearly been altered by the Grenvillian orogenic stress field. In order to assess their unique structural patterns it was necessary to eliminate the orogenic signature. From an analysis of regional geology alone, it is possible to narrow down the possible formation mechanisms of the Harvey Cardiff domes to diapirism. This is confirmed by foliations that appear consistent with the diapiric model. However, this interpretation is complicated by the fact that the domes appear to represent non horizontal slices through diapirs. As demonstrated by COMSOL modeling, this pattern can be explained by rotation of foliations subjected to pure or simple shear. Therefore, it is more likely that strain from the orogeny altered the expected diapiric foliation pattern. Although the model discussed in this study presented dome formation before the orogeny, it is also possible that the two events occurred simultaneously.

Lineations appear to have been overprinted by the orogen in the Cardiff Dome, but show a distinct pattern in the Cheddar Dome. The lack of shear sense indicators in the rocks at the hand sample and microscopic levels indicates that rocks were held at high enough temperatures after deformation to statically anneal.

The process of diapirism has not been linked to any particular stress states. This makes it difficult to gain information about the regional stress states during formation. However, it is significant that the Harvey Cardiff Domain domes were formed by the same mechanism as those in northern Québec. This indicates that similar conditions existed in both of these locations.

6. Acknowledgements

This project was funded by the Keck Geology Consortium, with supplemental funding from the Pomona College Geology Department. I would like to thank William Peck, Steven Dunn, and Michelle Markley, the project leaders of the Ontario Keck Geology Consortium Project, Summer 2011 for developing the foundation for this project and organizing field work. Thanks to all of my peers on the project for their help with field work, particularly Naomi Barshi and Calvin Mako. I

would also like to thank the professors at Pomona College Geology Department for their support and help in the development of this project. Thanks to Valbone Memeti for helping me with mineral identification, Eric Grosfils for constructing the COMSOL model and teaching me how to use it, Bob Gaines for his comments throughout the thesis process, and Linda Reinen for her encouragement and advise as my thesis advisor. Finally I would like to thank my peers at Pomona College Geology Department for their academic and emotional support.

7. References

Amato, J.M., Wright, J.E., Gans, P.B., and Miller, E.L., 1994, Magmatically induced metamorphism and deformation in the Kigluaik gneiss dome, Seward Peninsula, Alaska: Tectonics, v. 13, p. 515-527.

Bright, E.G., 1987, Precambrian geology of the Centre Lake Area Haliburton and Hastings Counties: Mine and Minerals Division, Ontario Geological Survey Open File Report 5658, p. 158.

Burger, H.R., Sheehan, A.F., and Jones, C.H., 2006, Introduction to Applied Geophysics: New York, W.W. Norton & Company, 554 p.

Carr S.D., Easton, R.M., Jamieson, R.A., and Culshaw, N.G., 2000, Geologic transect across the Grenville Orogen of Ontario and New York: Canadian Journal of Earth Sciences, V. 37, p. 193-216.

Cosca, M.A., Essene, E.J., and Mezger, K., 1995, Constraints on the duration of tectonic processes; protracted extension and deep-crustal rotation in the Grenville Orogen: Geology, v. 23, p. 361-364.

Culshaw, unpublished data, Lithology and Structure of Cheddar Area, 1 sheet.

Culshaw, N.G., 1981, Geological series, Precambrian geology of the Drag Lake area, Haliburton County, Southern Ontario; Ontario Geological Survey, Map P. 2404, scale 1:15,840, 1 sheet.

Darabi, M.H., and Piper, J.D.A., 2004, Paleomagnetism of the (late Mesoproterozoic) Stoer Group, northwest Scotland; implications for diagenesis, age and relationship to the Grenville, Orogeny: Geological Magazine, v. 141, p. 15-39.

Divi, R.R., and Fyson, W.K., 1973, Folds and Strain in Grenville Metamorphic Rocks, Bancroft, Ontario, Canada: Geological Society of America Bulletin, v. 84, p. 1607-1617.

Dixon, J.M., 1975, Finite strain and progressive deformation in models of diapiric structures: Tectonophysics, v. 28, p. 89-124.

Easton, R.M., and Kamo, S.L., 2011, Harvey-Cardiff Domain and its relationship to the Composite arc belt, Grenville Province; insights from U-Pb geochronology and geochemistry: Canadian Journal of Earth Science, v. 48, p. 347-370.

Eskola, P., 1949, The problem of mantled gneiss domes: Quarterly Journal of the Geological Society of London, V. 104, p. 461-476.

Fletcher, R.C., 1972, Application of a mathematical model to the emplacement of mantled gneiss domes: American Jourtnal of Science, v. 272, p. 197-216.

Gervais, F., Nadeau, L., and Malo, M., 2004, Migmatitic structures and solid-state diapirism in orothogneiss domes, eastern Grenville Province, Canada: Special Paper – Geological Society of America, v. 380, p. 359-378.

Gilbert, E., and Merle, O., 1987, Extrusion and radial spreading beyond a closing channel: Journal of Structural Geology, v. 9, p. 481-490.

Hanmer, S., 1988, Ductile thrusting at mid-crustal level, southwestern Grenville Province: Canadian Journal of Earth Sciences, v. 25, p. 1049-1059.

Hanmer, S., Corrigan, D., Pehrsson, S., and Nadeau, L., 2000, SW Grenville Province, Canada: the case against post-1.4 Ga accretionary tectonics: Tectonophysics, V. 319, p. 33-51.

Hanmer, S., and McEachern, S., 1992, Kinematical and rheological evolution of a crustal-scale ductile thrust zone, Central Medisedimentary Belt, Grenville orogen, Ontario: Canadian Journal of Earth Sciences, v. 29, p. 1779-1790.

Hewitt, D.F., 1957, Geology of Cardiff and Faraday townships: Annual Report – Ontario Department of Mines, v. 66, part 3.

Hodges, K.C., 2000, Tectonics of the Himalaya and southern Tibet from two perspectives: Geological Society of America Bulletin, v. 112, p. 324-350.

Kagan, Y.Y., and Jackson, D.D., 1991, Seismic gap hypotheses: Ten years after: Journal of Geophysical Research, v. 96, p. 419-421.

Lumbers, S.B. and Vertolli, V.M., 2000a, Precambrian geology, Gooderham area; Ontario Geological Survey, Preliminary Map P. 3405, scale 1:50,000, 1 sheet.

Lumbers, S.B. and Vertolli, V.M., 2000b, Precambrian geology, Burleigh Falls area; Ontario Geological Sruvey, Preliminary Map P.3404, scale 1:50,000, 1 sheet.

Lumbers, S.B. and Vertolli, V.M., 2003, Precambrian geology, Wilberforce area; Ontario Geological Survey, Preliminary Map P. 3526, scale 1:50,000, 1 sheet.

Makovsky, Y., Klemperer, S.L., Ratschbacher, L., and Alsdorf, D., 1999, Midcrustal reflector on INDEPTH wide-angle profiles: An ophiolitic slab beneath the India-Asia suture in southern Tibet?: Tectonics, v. 18, p. 793-808.

Martínez- Martínez, J.M., Soto, J.I., and Balanyá, J.C., 2002, Orthogonal folding of extensional detachments: Structure and origin of the Sierra Nevada elongated dome (Betics, SE Spain): Tectonics, v. 21, p. 1-20.

McNeice, G.W., Boerner, D.E., Kurtz, R.D., and Jones, A.G., 1991, Gravity studies at the Lemieux Dome, Gaspé, Québec: Geological Survey of Canada Open File Report 2291, 31 p.

Ontario Geologic Survey, Bedrock Geology: http://www.mndm.gov.on.ca/mines/ogs_earth_e.asp (accessed April 2012).

Passchier, C.W., and Trouw, R.A.J., 2005, Microtectonics: New York, Springer, 366 p.

Pêcher, A., and Le Fort, P., 1999, Late Miocene tectonic evolution of the Karakororam-Nanga Parbat contact zone (northern Pakistan): Special Paper – Geological Society of America, v. 328, p. 145-158.

Rivers, T., 1997, Lithotectonic elements of the Grenville Province: review and tectonic implications: Precambrian Research, v. 86, p. 117-154.

Rivers, T., 2008, Assembly and preservation of lower, mid, and upper orogenic crust in the Grenville Province; implications for the evolution of large hot long duration orogens: Precambrian Research, v. 1967, p. 237-259.

Timmerman, H., Parrish, T.T., Jamieson, R.A., and Culshaw, N.G., 1997, Time of metamorphism beneath the Central Metasedimentary Belt boundary thrust zone, Grenville Orogen, Ontario; accretion at 1080 Ma? Canadian Journal of Earth Sciences, v. 34, p. 1023-1029.

Tollo, R.P., Corriveau, L., McLelland, J., and Bartholomew, M.J., 2004, Proterozoic tectonic evolution of the Grenville orogen in North America: An introduction: Geological Society of America Memoir, v. 197, p. 1-18.

Tollo, R.P, et al., 2004, Petrologic and geochronologic evolution of the Grenville orogen, northern Blue Ridge Province, Virginia: Geological Society of America Memoir, v. 197, p. 647-677.

Teyssier, C., and Whitney, D.L., 2002, Gneiss domes and orogeny: Geology, v. 30, p. 1139-1142.

Van der Pluijm, B.A., Marshak, S., 2004, Earth Structure: New York, W.W. Norton, 656 p.

Van Staal, C.R., and Williams, P.F., 1983, Evolution of a Svecofennian mantled gneiss dome in SW Finland, with evidence for thrusting: Precambrian Research, v. 21, p. 101-128.

Wernicke, B., and Axen, G.J., 1988, On the role of isostasy in the evolution of normal fault systems: Geology, v. 16, p. 848-851.

Whitney, D.L., Teyssier, C., and Vanderhaeghe, O., 2004, Gneiss domes and crustal flow: Special Paper – Geological Society of American, v. 380, p. 15-33.

Yin, A., 2004, Gneiss domes and gneiss dome systems: Special Paper – Geological Society of America, v. 380, p. 1-14.

Appendix A: Structural Measurements

All averages were calculated using the mean vector calculation on Stereo32.

Latitude	Longitude						
-78.213	44.984						
		Foliation			Lineation		
		Dip Direction	Dip		Trend	Plunge	Type
		124	59		115	59	Mineral
		134	64		136	61	Mineral
		130	53		125	53	Mineral
		140	57		138	60	Mineral
		118	61	Average	128	59	Mineral
		141	58		180	33	Fold Hinge
		Average 131	59		190	40	Fold Hinge
				Average	185	37	Fold Hinge
-78.157	44.993						
		186	76		103	25	Mineral
		181	65		103	29	Mineral
		Average 184	70	Average	103	27	Mineral
					118	46	Hinge
					140	56	Hinge
					64	86	Hinge
				Average	125	34	Hinge
-78.233	44.986						
		101	80		120	42	Mineral
		114	51				
		141	45				
		92	52				
		Average 110	56				
-78.133	44.911						
		41	81		138	38	Mineral
		38	83		125	30	Mineral
		48	56		122	46	Mineral
		44	74		111	44	Mineral
		47	76		125	31	Mineral
		49	78		127	42	Mineral
		39	78	Average	125	39	Mineral
		42	70				
		41	80				
		42	84				
		Average 43	76				

-78.14	44.947						
		173	80				
		172	63				
		186	52				
		165	65				
		187	54				
		Average 176	63				
-78.216	44.985						
		127	71		111	70	Mineral
		130	55		95	55	Mineral
		127	71	Average	101	63	Mineral
		118	60		13	20	Boudin Neck
		Average 125	64				
-78.238	44.95						
		112	66		65	60	Mineral
		103	65		60	80	Mineral
		111	74	Average	64	70	Mineral
		Average 109	68				
-78.146	44.91						
		122	34				
-78.13	44.91						
		150	28				
-78.107	44.935						
		22	83				
-78.112	44.972						
		290	71				
-78.162	44.994						
		166	69				
-78.124	44.897						
		140	41				
-78.101	44.938						
		100	42				
-78.105	44.906						
		136	35				
-78.175	44.992						
		152	72		134	74	Mineral
-78.104	44.937						
		85	41		94	44	Mineral

Appendix B: Sample Descriptions

Images of thin sections can be found in Appendix C

Sample	Thin Section	Rock Type	Latitude	Longitude
11CS001	Y	granitic gneiss	44° 54.524	-78° 9.266
11CS002	Y	amphibolite	44° 54.616	-78° 8.774
11CS003	Y	biotite schist	44° 54.755	-78° 7.496
11CS004	Y	pegmatite	44° 54.879	-78° 7.203
11CS005	Y	marble	44° 55.873	-78° 7.191
11CS006	Y	amphibolite	44° 56.089	-78° 6.418
11CS007	Y	amphibolite	44° 59.450	-78° 7.980
11CS008	N	amphibolite	44° 59.450	-78° 7.980
11CS009	Y	granitic gneiss	44° 56.872	-78° 8.407
11CS010	Y	amphibolite	44° 56.872	-78° 8.407
11CS011	Y	amphibolite	44° 56.872	-78° 8.407
11CS012	N	marble	44° 59.594	-78° 9.739
11CS013	Y	granite	44° 59.594	-78° 9.739
11CS014	Y	amphibolite	44° 59.100	-78° 12.944
11CS015	Y	amphibolite	44° 59.100	-78° 12.944
11CS016	Y	amphibolite	44° 59.100	-78° 12.944
11CS017	Y	amphibolite	44° 59.100	-78° 12.944
11CS018	N	amphibolite	44° 59.100	-78° 12.944
11CS019	Y	amphibolite	44° 57.000	-78° 14.280
11CS020	Y	amphibolite	44° 57.000	-78° 14.280
11CS021	Y	amphibolite	44° 53.808	-78° 7.395
11CS022	N	amphibolite	44° 56.198	-78° 6.190
11CS023	Y	amphibolite	44° 56.198	-78° 6.190
11CS024	Y	amphibolite	44° 59.450	-78° 7.980
11CS025	Y	amphibolite	44° 59.450	-78° 7.980
11CS026	Y	amphibolite	44° 56.268	-78° 6.056
11CS027	Y	amphibolite	44° 56.268	-78° 6.056

Appendix C: Thin Section Photographs

All thin sections are 40μm thick and photographed under cross-polarized light.

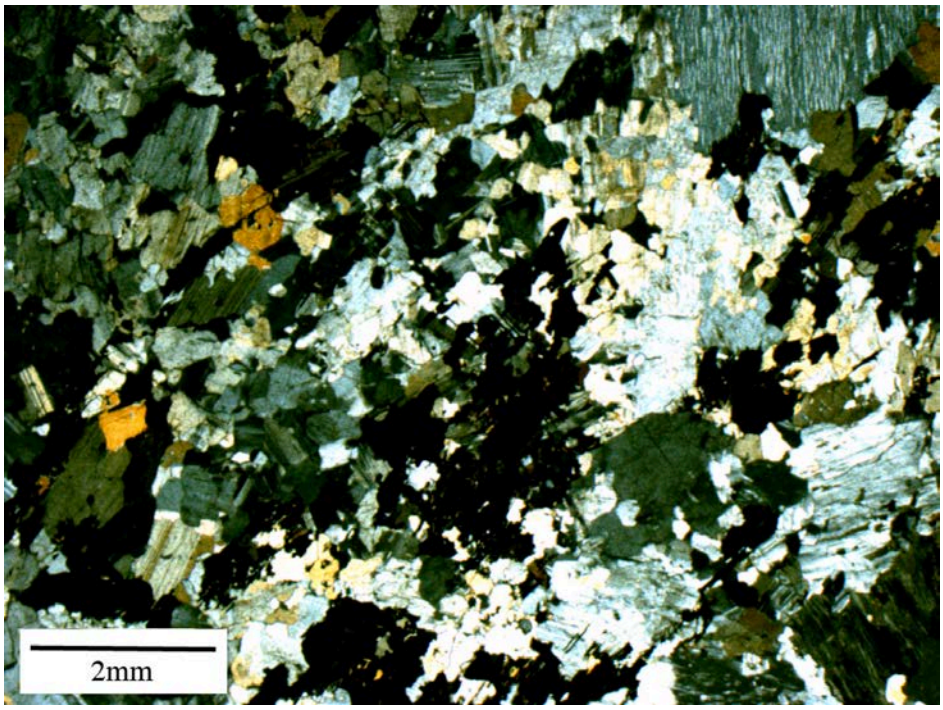

Figure C1: 11CS001

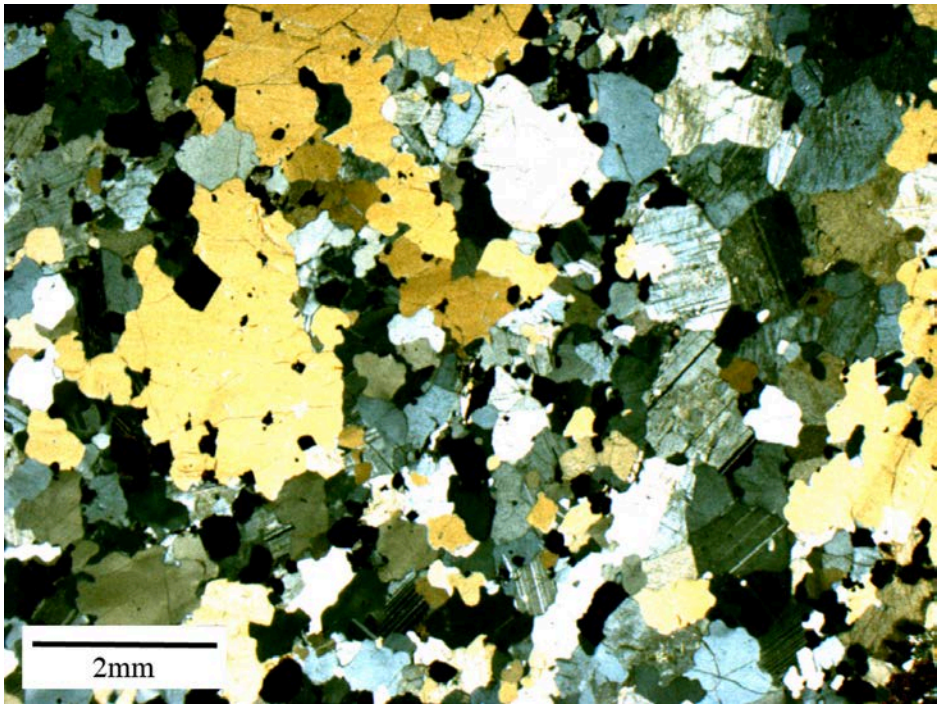

Figure C2: 11CS002

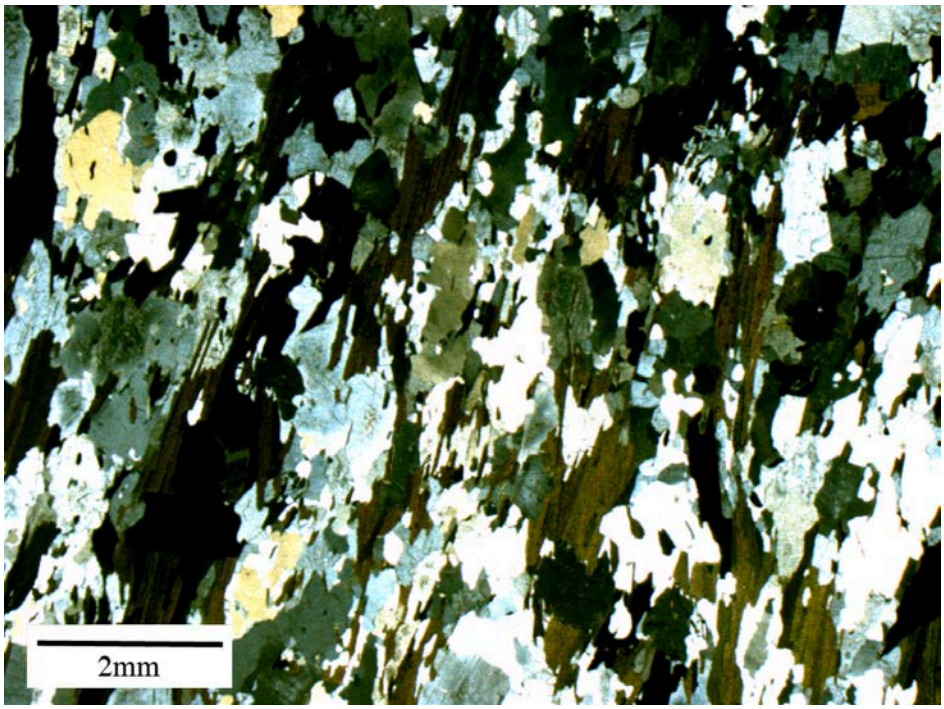

Figure C3: 11CS003

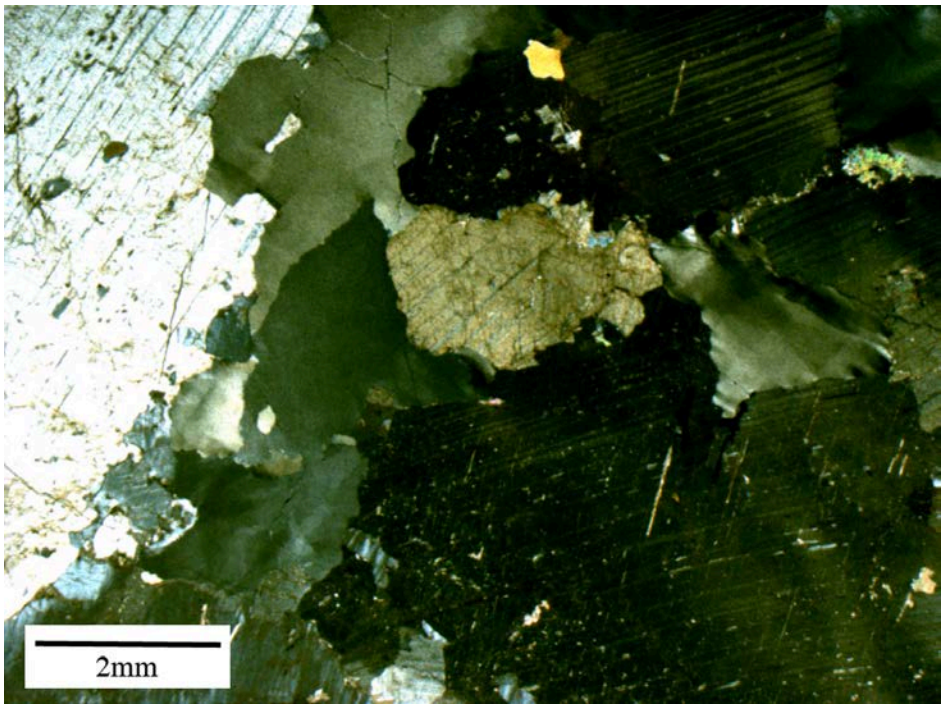

Figure C4: 11CS004

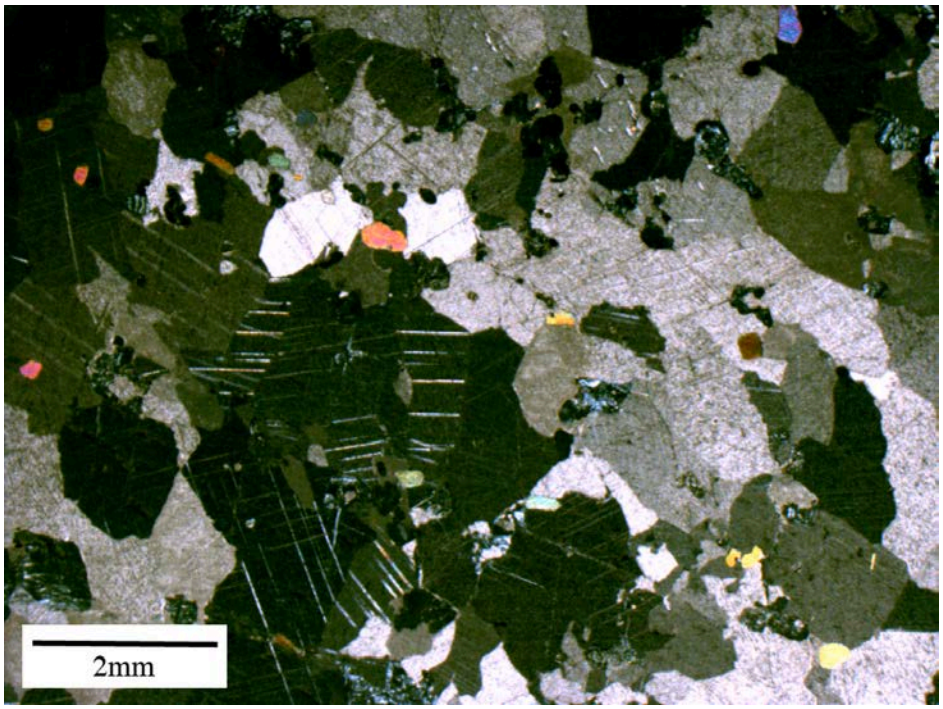

Figure C5: 11CS005

Figure C6: 11CS006

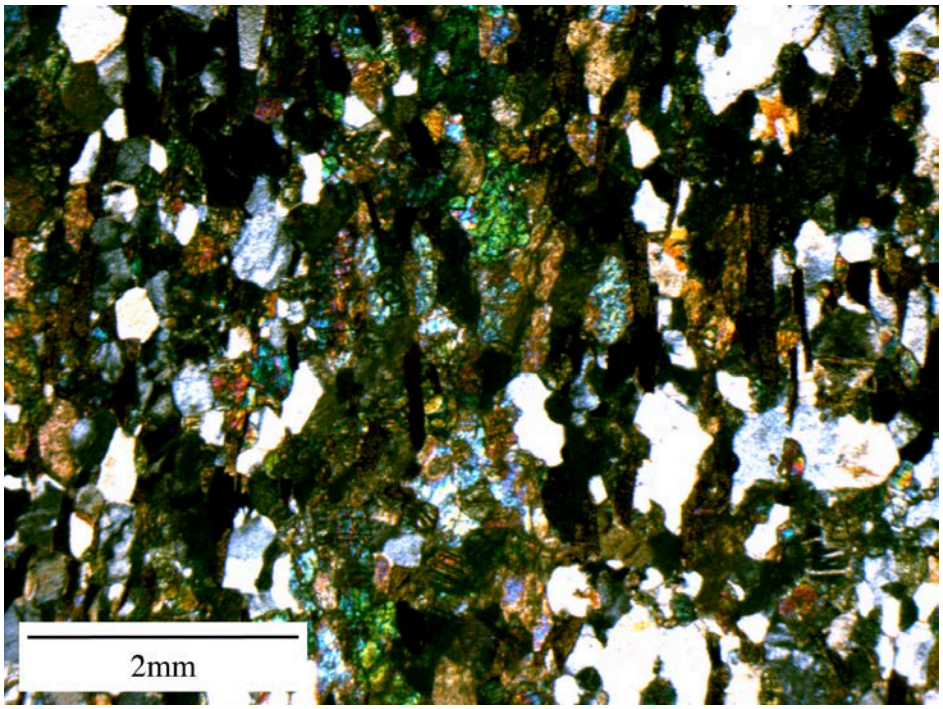

Figure C7:11 CS007

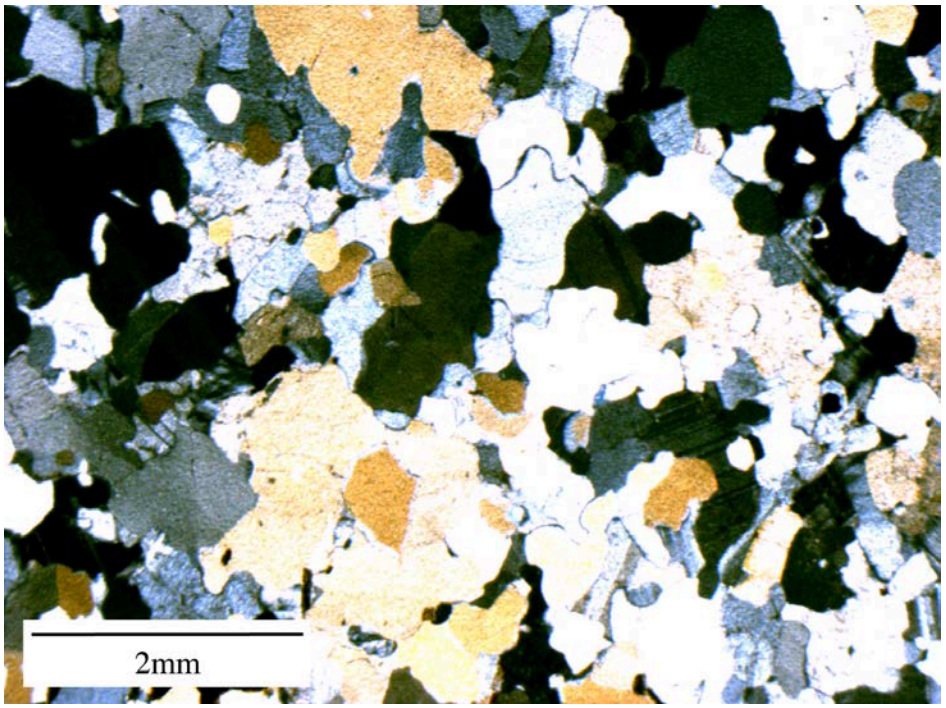

Figure C8: 11CS009

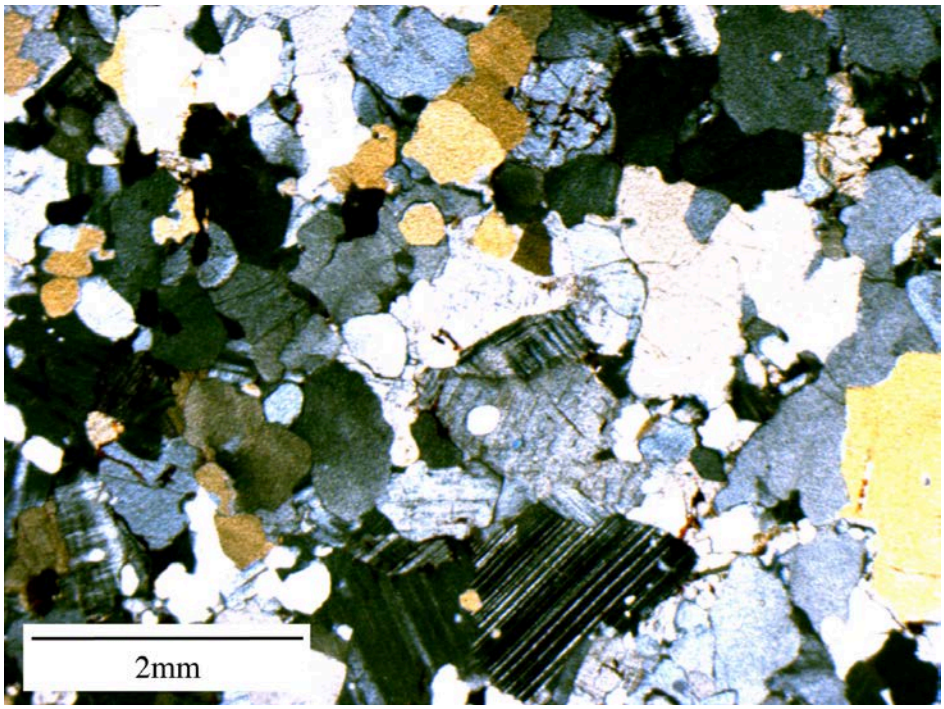

Figure C9: 11CS010

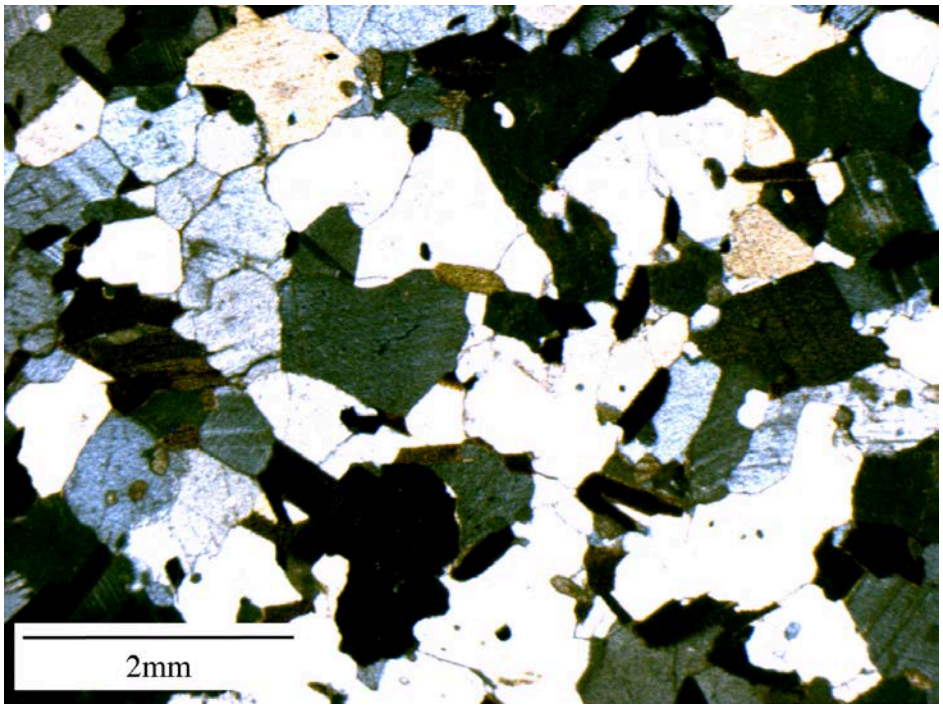

Figure C10:11CS011

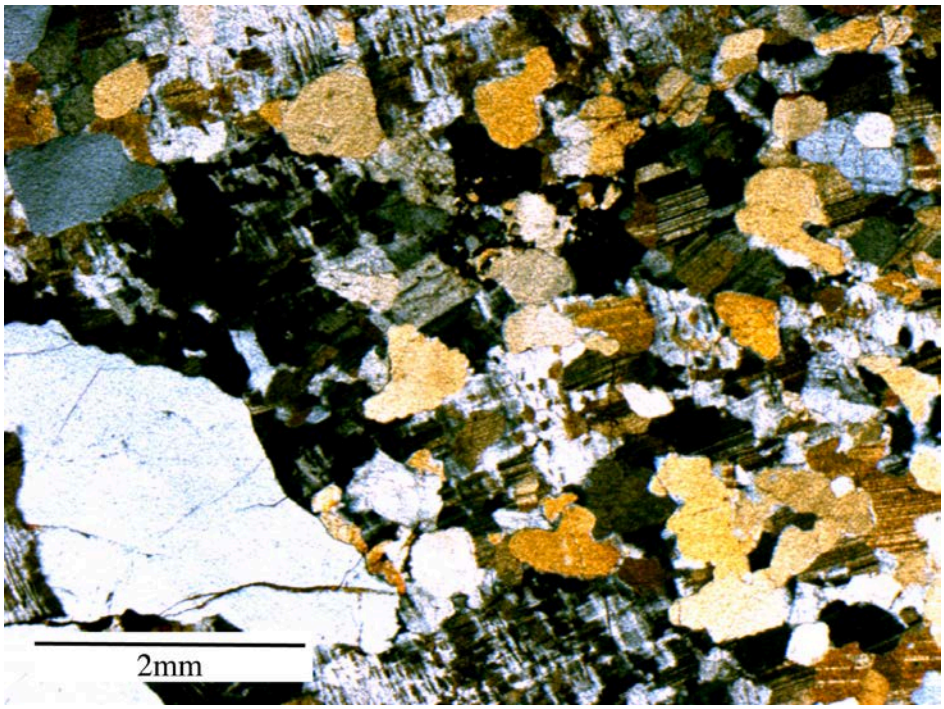

Figure C11: 11CS013

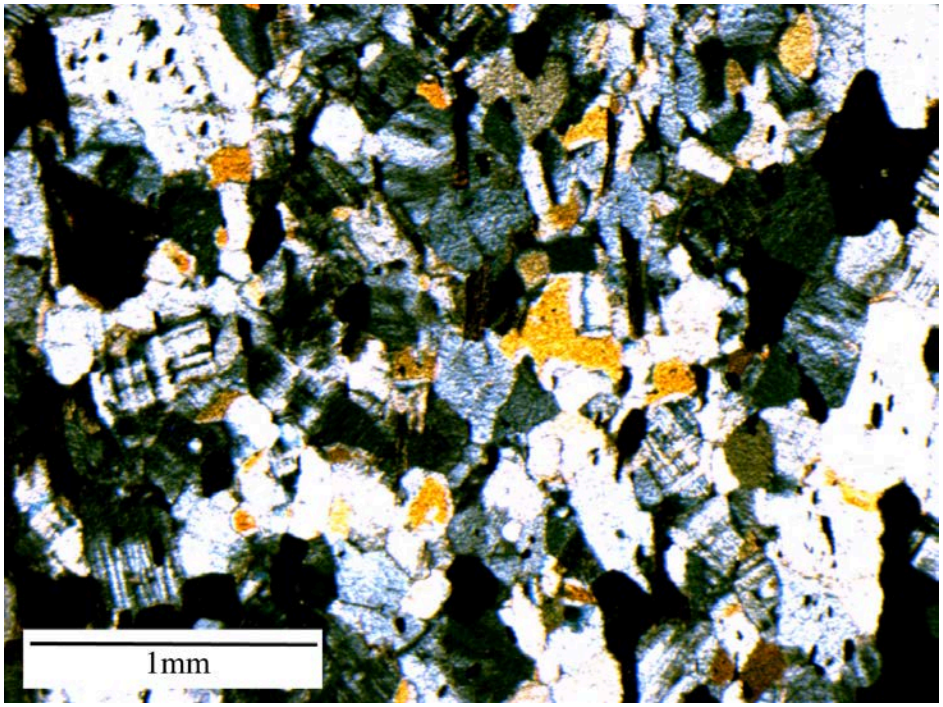

Figure C11: 11CS014

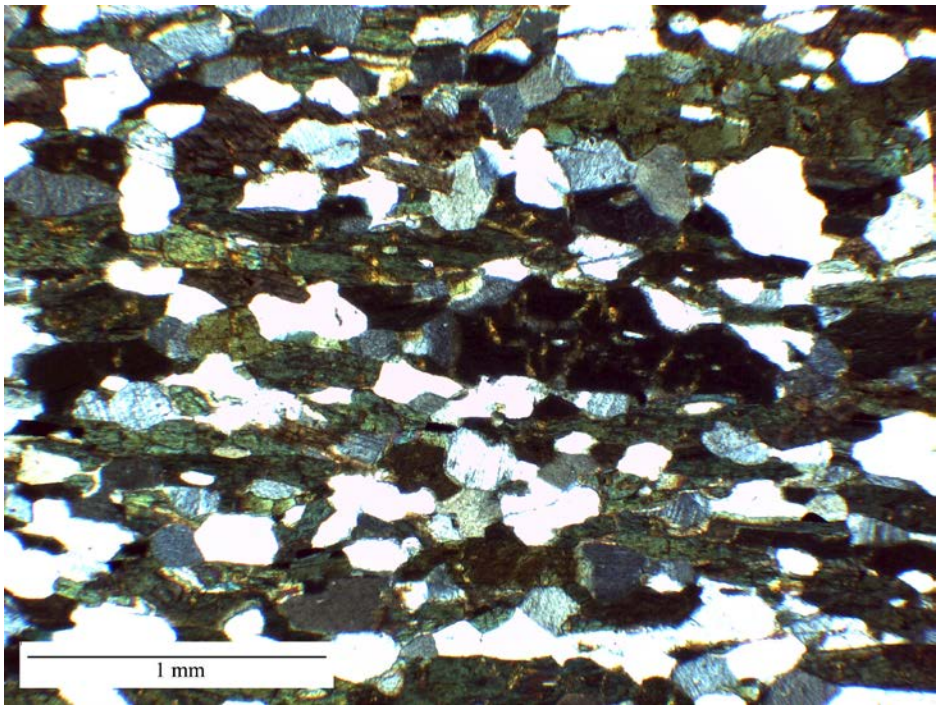

Figure C12: 11CS015

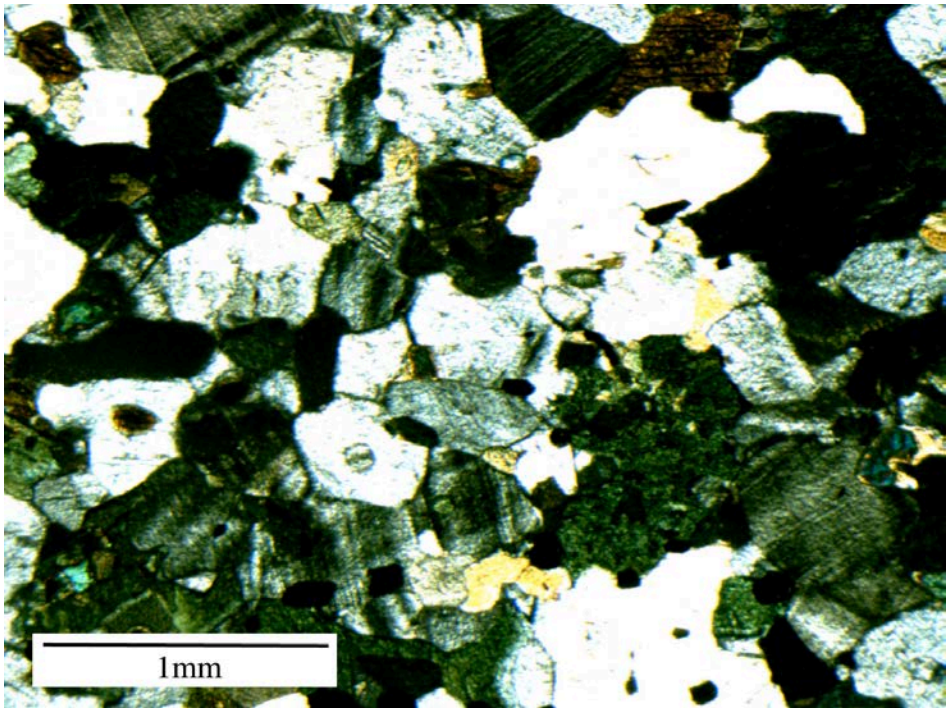

Figure C13: 11CS016

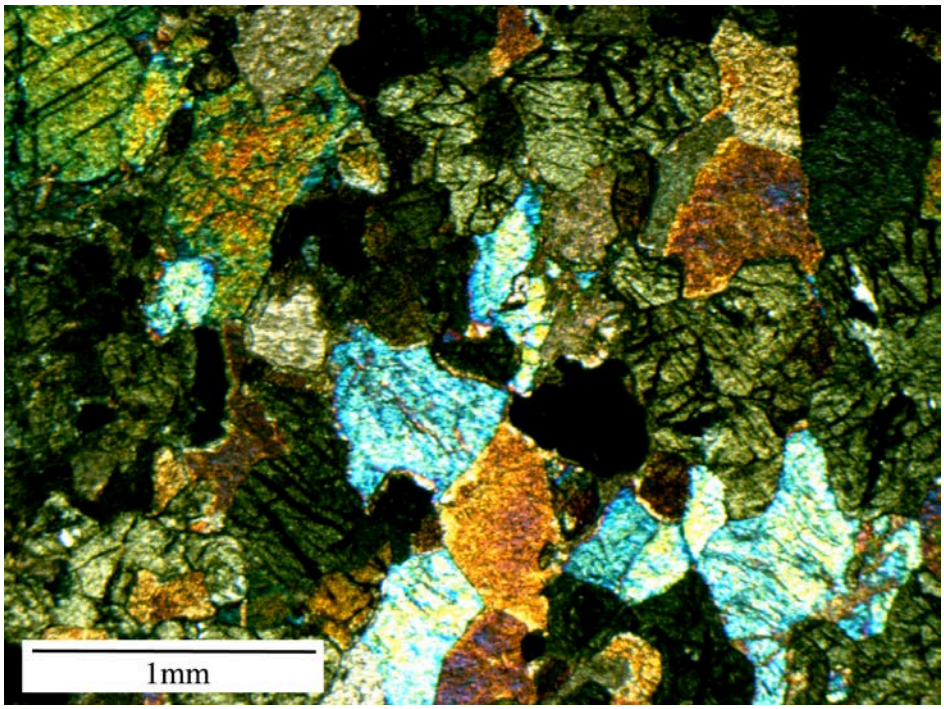

Figure C14: 11CS017

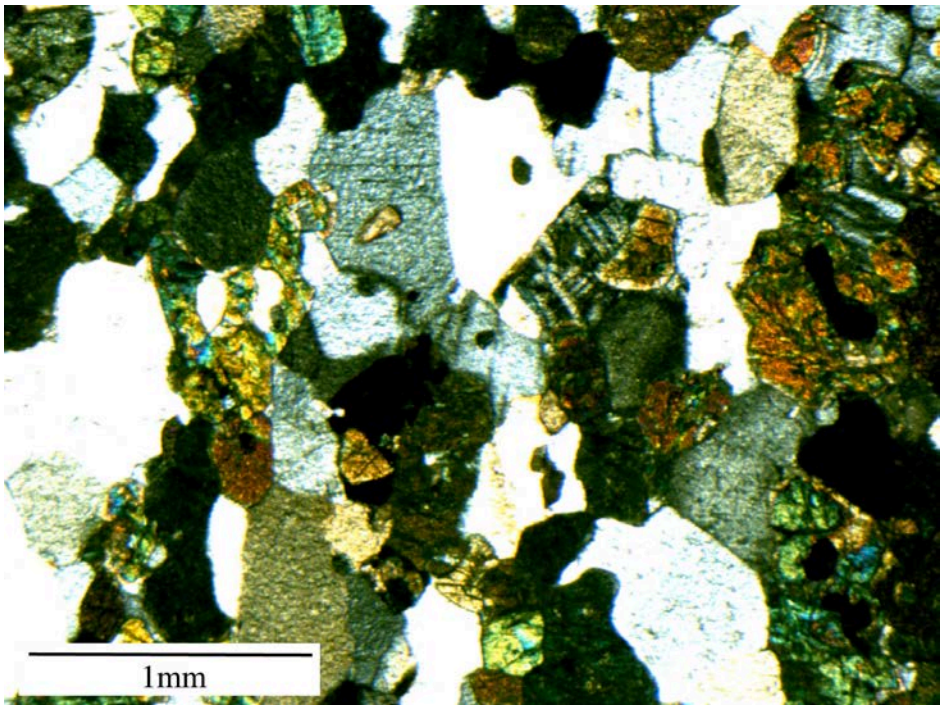

Figure C15: 11CS019

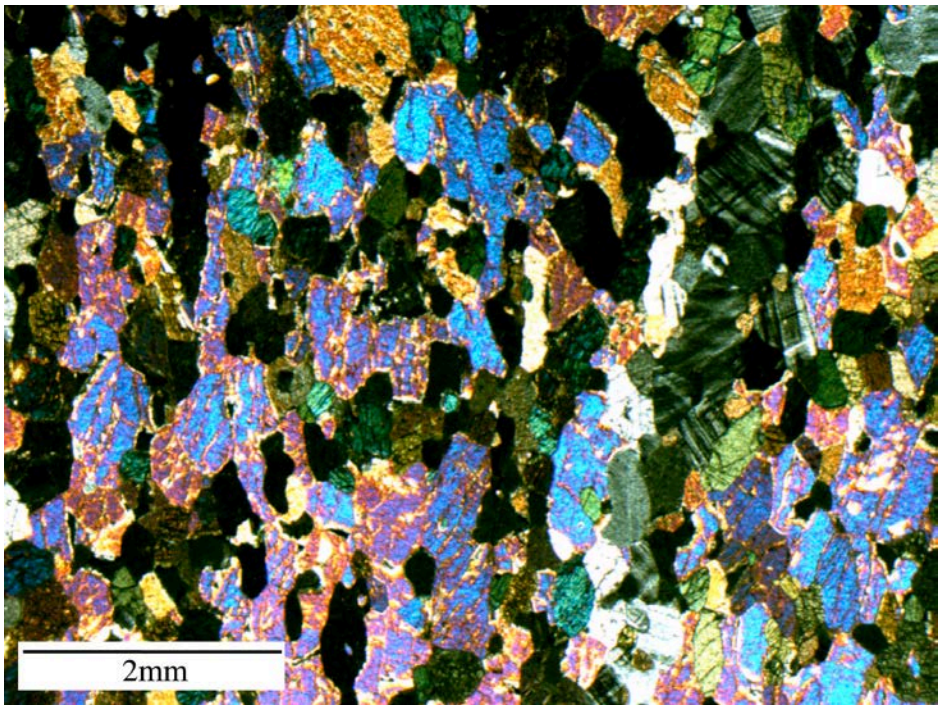

Figure C16:11CS020

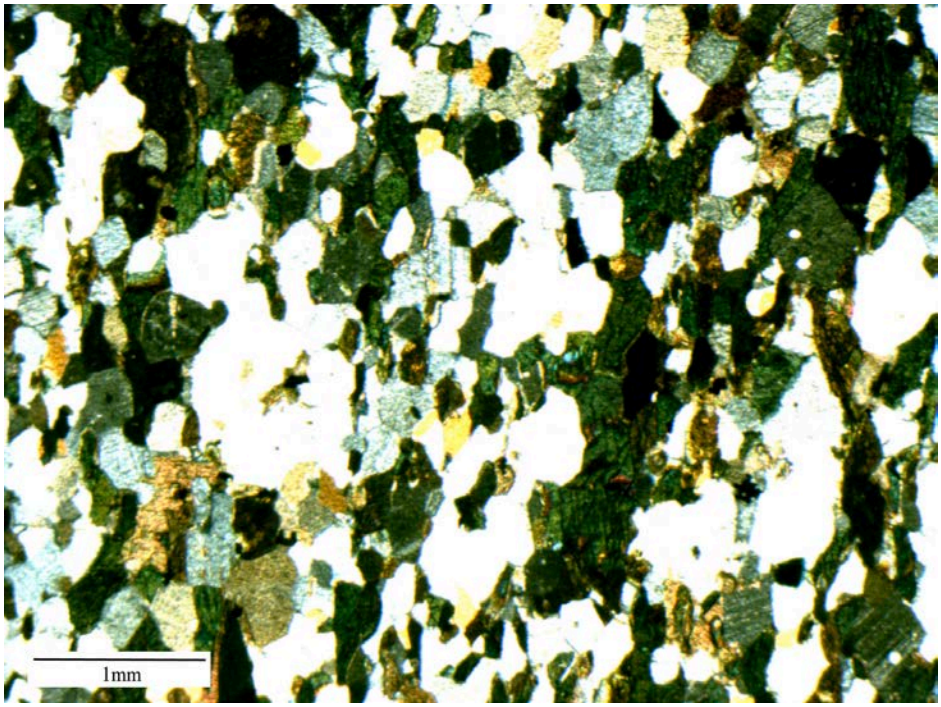

Figure C17: 11CS021

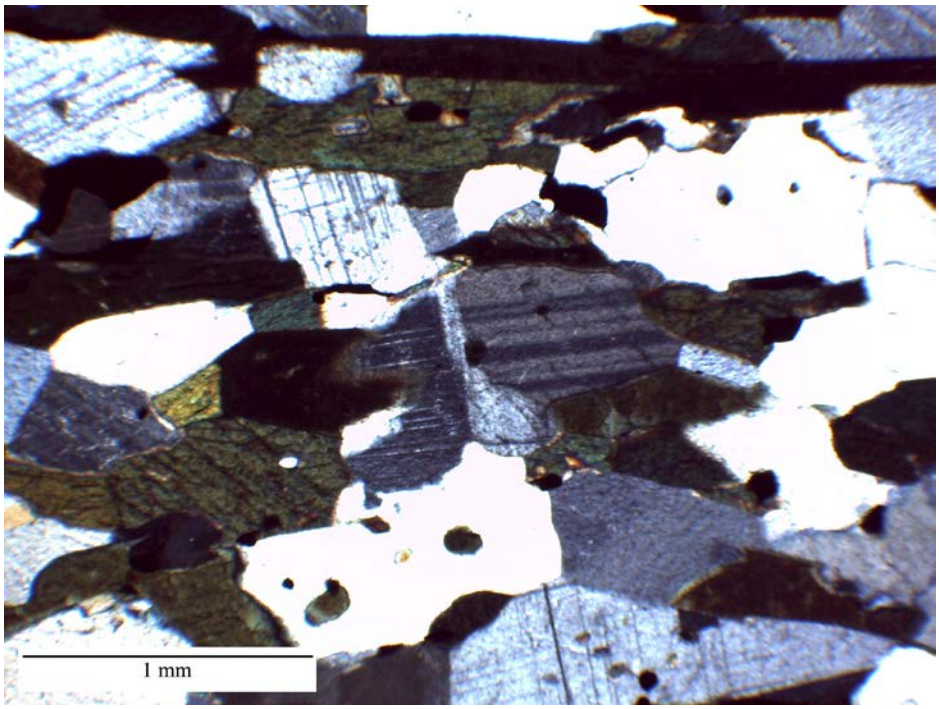

Figure C18: 11CS023

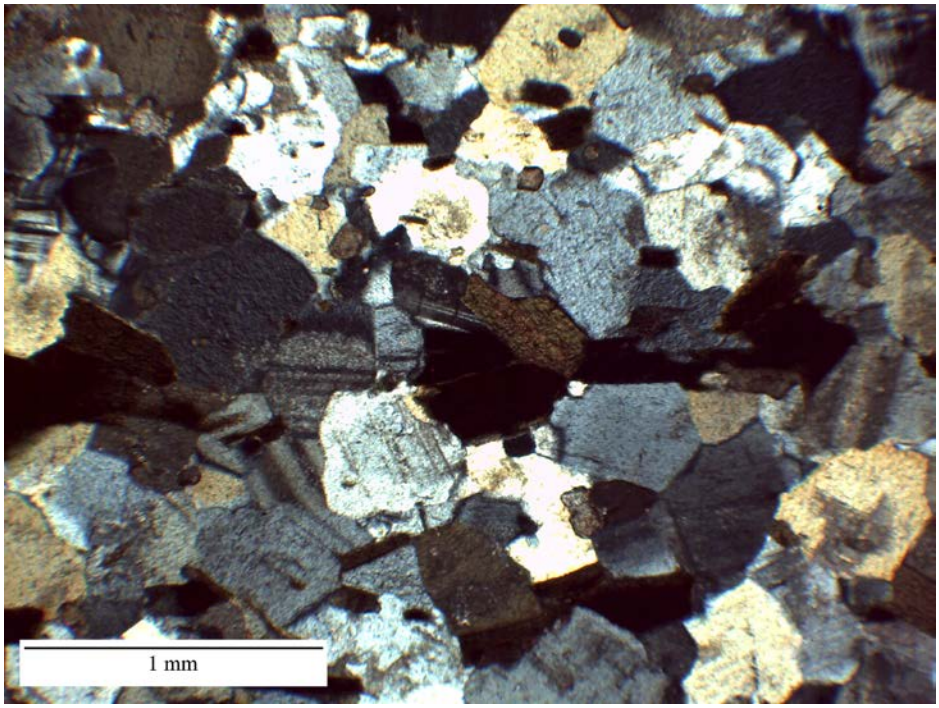

Figure C19: 11CS024

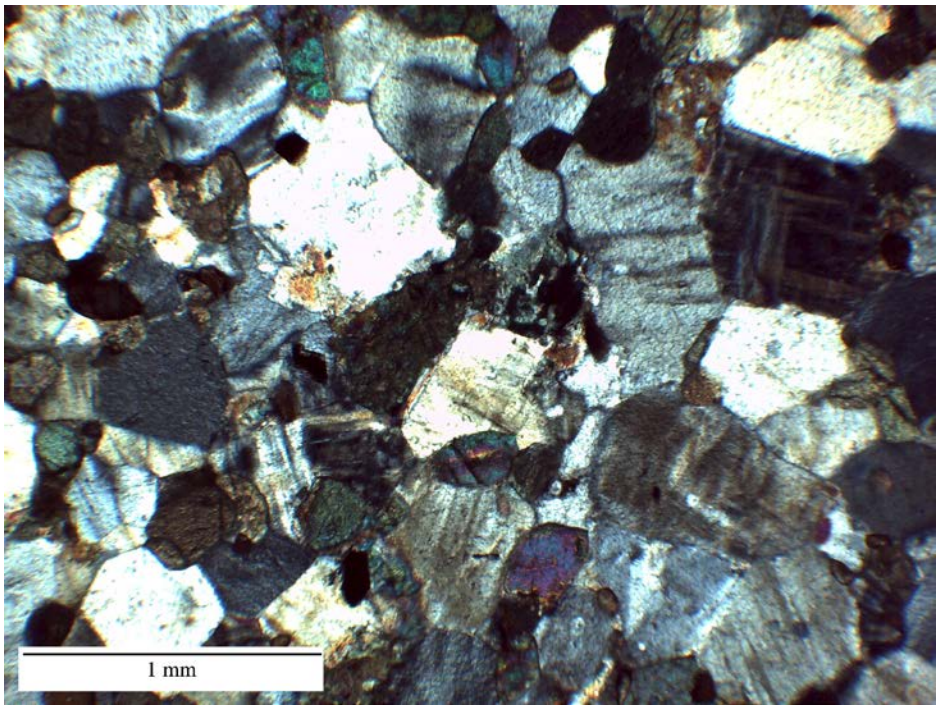

Figure C20: 11CS025

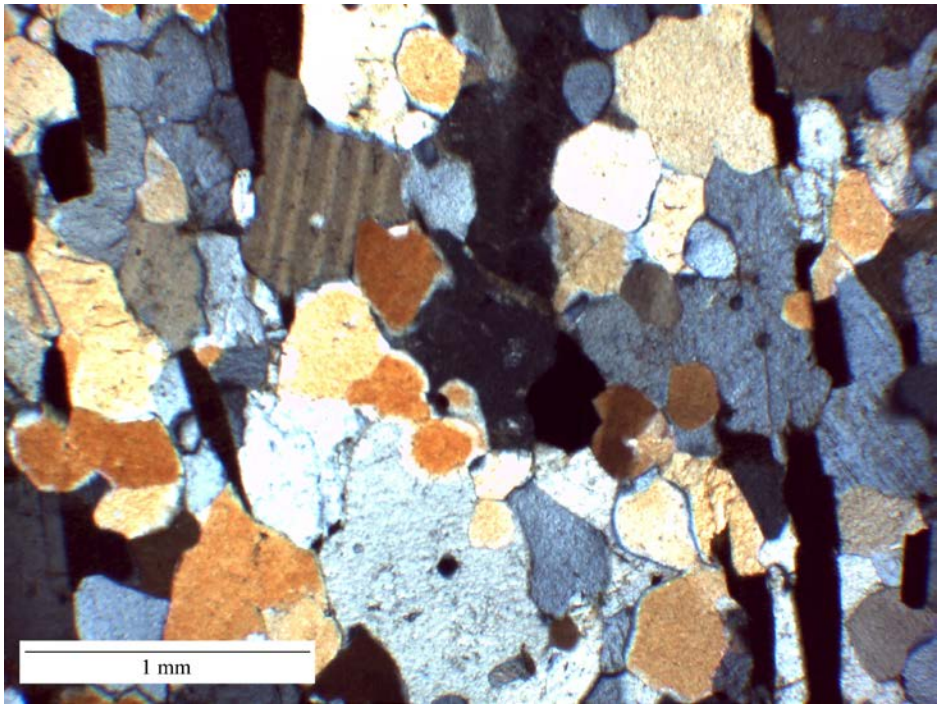

Figure C21: 11CS026

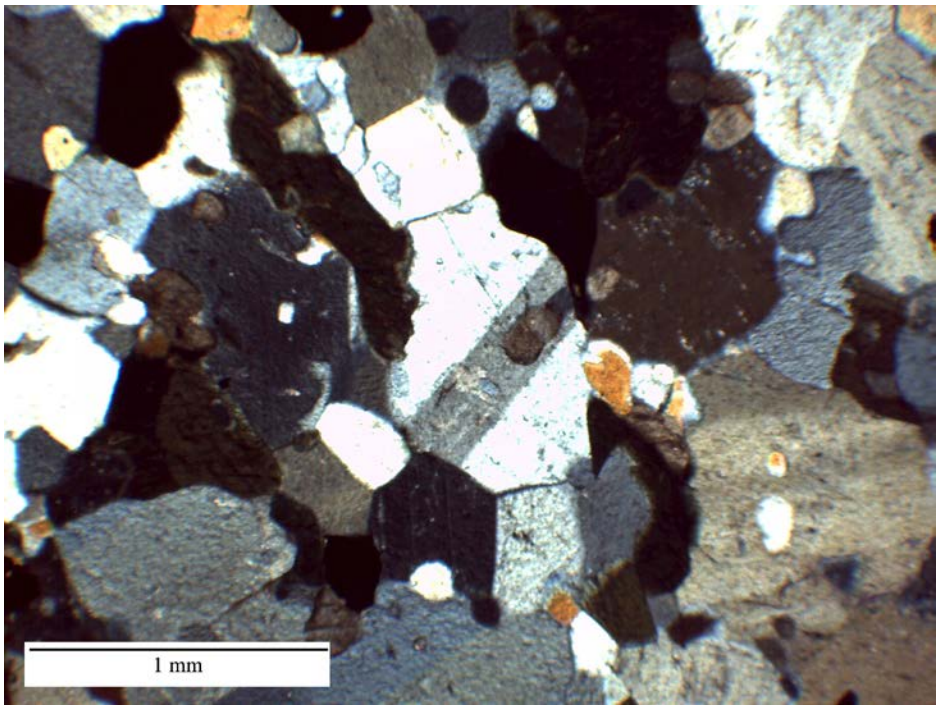

Figure C22: 11CS027

Appendix D: Dome System Analysis

Shushwap Complex Gneiss Domes: Evenly Spaced

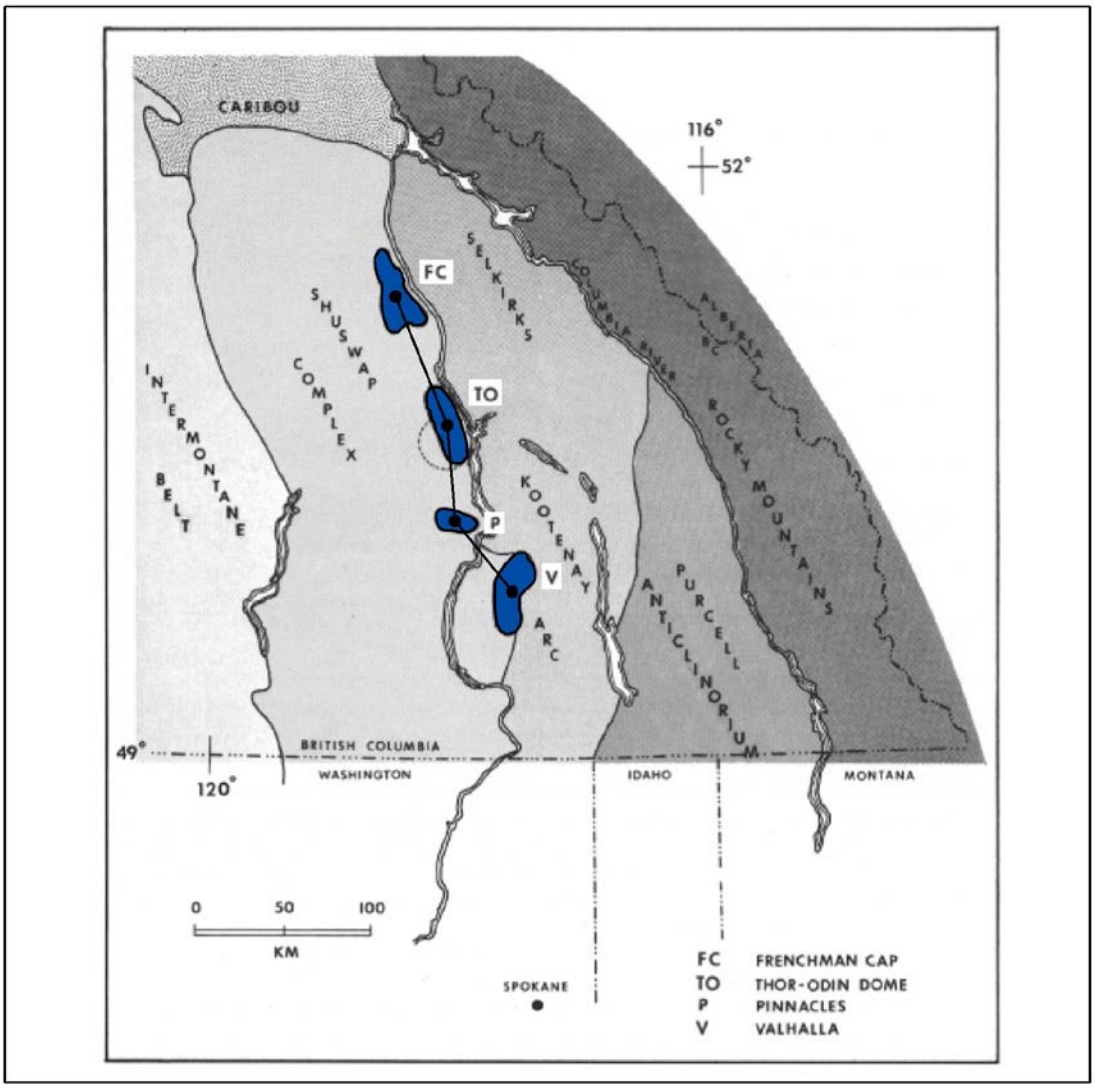

Figure D1: Evenly Spaced Domes of the Shuswap Complex. Gneiss domes polygons are blue, and centroids are marked with black dots.

Table D1: Spacing Calculations for Shuswap Complex

Distance Between Centers	Average (km)	Standard Deviation	Coefficient of Variation
79 km	62 km	15	0.24
54 km			
52 km			

North Himalaya Gneiss Domes: Unevenly Spaced

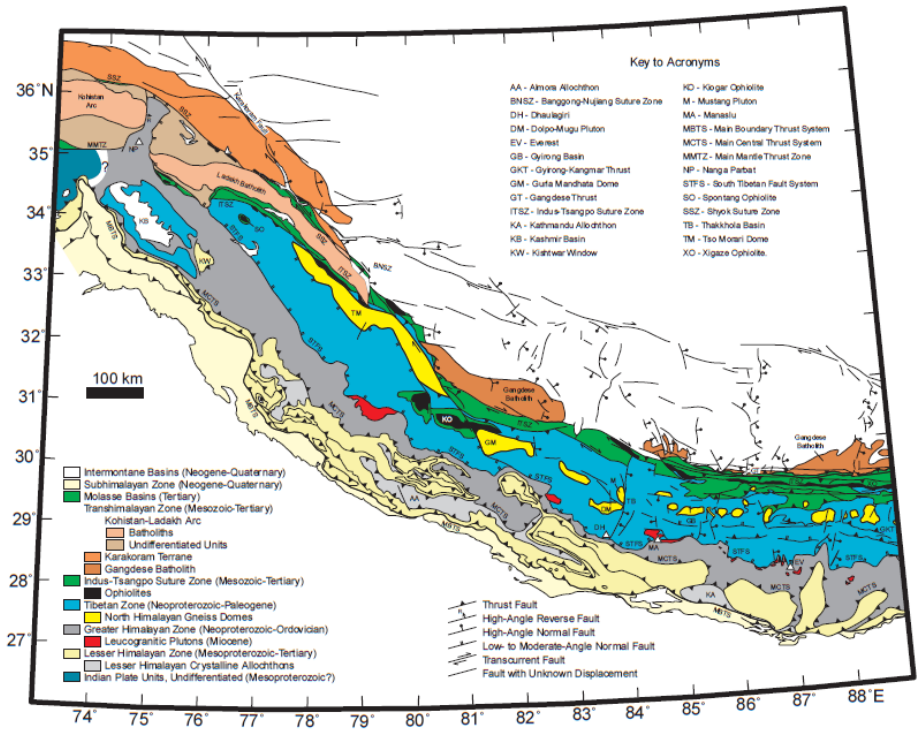

Figure D2: Geologic map of the North Himalaya Gneiss Domes. Gneiss domes are mapped in yellow. Distances were traced between geometric centroids.

The gneiss domes in this system vary from tens to hundreds of km in length/diameter. A clear linear array of domes appears to the east of the high angle normal fault. To the northwest are a series of larger domes with a more northerly strike. The mapped dome farthest to the west does not fall under the criteria of circular. Below are the distances between dome centers, beginning on the east side of the complex. There are three sets of calculations: one including only those domes east of the fault, one including all domes except for the one farthest to the west, and one including all domes.

Table D2: Spacing Calculations for Northern Himalaya Gneiss Domes

Distance Between Centers	Average	Standard Deviation	Coefficient of Variation
139 km			
80 km			
34 km			
76 km			
25 km			
34 km			
34 km			
20 km			
27 km			
24 km			
44 km			
69 km	51 km	35 km	0.69
37 km			
39 km			
15 km			
27 km	45 km	32 km	0.70
231 km	56 km	54 km	0.97

Appendix E: COMSOL Model Details

This appendix describes the steps of creating the COMSOL model in full detail. The goal was to create a model that applied pure and shear strain orthogonal to the dip of the regional foliation. First, I created a rectangle of material representing the mantle rocks (see Table E3 for values of model construction parameters and Tables E1 and E2 for elastic parameters). For each model, the edges of the material block were given different allowances for movement. A circle representing the gneiss dome is centered within this block and has the elastic properties of granite. Passive ellipses representing foliation lie along a horizontal plane representing the ground surface. I measured the exact dip angles on each ellipse and interpolated foliation values from Dixon's analogue models for comparison (1975).

In order to create pure and simple shear in the COMSOL model space, displacement was applied to the top horizontal face of the rectangle. Because the goal was to apply strain orthogonal to the dip of regional foliation, the entire model was rotated twenty degrees counter clockwise (Fig. E1). In the bulk of the text, this rotation was removed for simplicity by rotating the model and results back to their original orientation.

In order to create strain within the block, I applied different constraints on the movements of each of the block walls (See Fig. E1 for numbering system). In the pure shear regime wall 1 was given a prescribed displacement in the negative y direction, walls 3 and 4 were allowed to grow or shrink in length by applying a roller condition. I allowed wall 2 to move freely in order to maintain conservation of volume in the block. In the simple shear regime, I applied a prescribed displacement in the negative x direction to wall 1. Walls 2 and 4 were left free to compensate for strain, and wall 3 was fixed in place (see Table E4 for displacement and strain values).

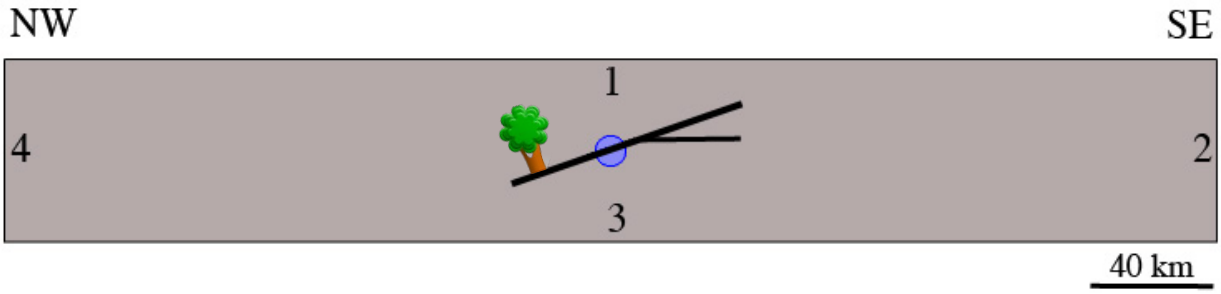

Figure E1: Schematic of COMSOL model setup. The ground surface was rotated 20 degrees in order to make the regional foliation plane parallel with horizontal surface 1 to which stress was being applied. The surfaces of the model are numbered 1-4 to simplify explanation of boundary conditions in the text.

Table E1: Determination of Elastic Properties of the Mantle

	Density (km/m^3)	Young's Modulus (Pa)	Poisson's Ratio
Limestone	2.44	33.7e9	.156
Basalt	2.74	63.0 e9	.220
Andesite	2.57	54.0 e9	.180
Average	**2.6**	**52 e9**	**.56**

Table E2: Elastic Property Parameters

Dome Density	2650 kg/m^3
Dome Young's Modulus	40e9 Pa
Dome Poisson's Ratio	.7
Mantle Density	2600 km/m^3
Mantle Young's Modulus	52e9 Pa
Mantle Poisson's Ratio	.56

Table E3: Model Construction Parameters

Height of Block	60 km
Width of Block (Pure Shear)	400 km
Width of Block (Simple Shear)	2000 km
Radium of Dome	5 km
Short Axis of Ellipse	125 m
Long Axis of Ellipse	500 m

Table E4: Displacement Parameters

Displacement (Pure Shear)	9000 m
Displacement (Simple Shear)	9000 m
Longitudinal Strain (Pure Shear)	.15
Shear Strain (Simple Shear)	.15